Brain Struct Funct (2017) 222:2603–2624
DOI 10.1007/s00429-016-1360-4

ORIGINAL ARTICLE

Bipolar cell gap junctions serve major signaling pathways in the human retina

Orsolya Kántor[1,2,3] · Alexandra Varga[3] · Roland Nitschke[4,5] · Angela Naumann[4,5] · Anna Énzsöly[3,6] · Ákos Lukáts[3] · Arnold Szabó[3] · János Németh[6] · Béla Völgyi[2,7,8,9]

Received: 29 June 2016 / Accepted: 22 December 2016 / Published online: 10 January 2017

Abstract Connexin36 (Cx36) constituent gap junctions (GJ) throughout the brain connect neurons into functional syncytia. In the retina they underlie the transmission, averaging and correlation of signals prior conveying visual information to the brain. This is the first study that describes retinal bipolar cell (BC) GJs in the human inner retina, whose function is enigmatic even in the examined animal models. Furthermore, a number of unique features (e.g. fovea, trichromacy, midget system) necessitate a reexamination of the animal model results in the human retina. Well-preserved postmortem human samples of this study are allowed to identify Cx36 expressing BCs neurochemically. Results reveal that both rod and cone pathway interneurons display strong Cx36 expression. Rod BC inputs to AII amacrine cells (AC) appear in juxtaposition to AII GJs, thus suggesting a strategic AII cell targeting by rod BCs. Cone BCs serving midget, parasol or koniocellular signaling pathways display a wealth of Cx36 expression to form homologously coupled arrays. In addition, they also establish heterologous GJ contacts to serve an exchange of information between parallel signaling streams. Interestingly, a prominent Cx36 expression was exhibited by midget system BCs that appear to maintain intimate contacts with bistratified BCs serving other pathways. These findings suggest that BC GJs in parallel signaling streams serve both an intra- and inter-pathway exchange of signals in the human retina.

Keywords Gap junction · Electrical synapse · Bipolar cell · Magnocellular pathway · Parvocellular pathway · Koniocellular pathway

Introduction

Gap junctons (GJ) in the central nervous system connect interneurons into electrical syntitia to serve signal correlation. Correlated signals then may enhance saliency of information. In this scheme synchronized inputs to a common neuronal target are more effective than their unsynchronized counterparts (Alonso et al. 1996; Usrey and

Electronic supplementary material The online version of this article (doi:10.1007/s00429-016-1360-4) contains supplementary material, which is available to authorized users.

✉ Béla Völgyi
volgyi01@gamma.ttk.pte.hu; volgyb01@med.nyu.edu

[1] Department of Neuroanatomy, Faculty of Medicine, Institute for Anatomy and Cell Biology, University of Freiburg, 79104 Freiburg, Germany

[2] MTA-PTE NAP B Retinal Electrical Synapses Research Group, Pécs 7624, Hungary

[3] Department of Anatomy, Histology and Embryology, Semmelweis University, Budapest 1094, Hungary

[4] Life Imaging Center, Center for Biological Systems Analysis, University of Freiburg, 79104 Freiburg, Germany

[5] BIOSS Centre for Biological Signaling Studies, University of Freiburg, 79104 Freiburg, Germany

[6] Department of Ophthalmology, Semmelweis University, Budapest 1085, Hungary

[7] Department of Experimental Zoology and Neurobiology, University of Pécs, Pécs 7624, Hungary

[8] János Szentágothai Research Center, University of Pécs, Ifjúság street 20, Pécs 7624, Hungary

[9] Department of Ophthalmology, New York University Langone Medical Center, New York, NY 10016, USA

Reid 1999). Retinal interneurons have also been reported to utilize GJs as well to serve postsynaptic ganglion cells (GCs) with synchronous inputs (reviewed by Bloomfield and Völgyi 2009; Völgyi et al. 2013a). Connexin36 (Cx36) is the most prominent GJ protein in the nervous system and it has also been reported to underly the transmission, averaging and correlation of retinal signals prior conveying visual information to the brain. Whereas Cx36 and Cx45 have been found in both plexiform layers (Güldenagel et al. 2000; Petrasch-Parwez et al. 2004), others are restricted to either the outer (OPL) or the inner plexiform layer (IPL) including Cx50, Cx57 and Cx30.2 (Massey et al. 2003; Hombach et al. 2004; Müller et al. 2010). Cx36 and Cx45 have been shown to process rod-mediated signals (Feigenspan et al. 2001, 2004; Güldenagel et al. 2001; Mills et al. 2001; Deans et al. 2002; Lee et al. 2003; Völgyi et al. 2004; Han and Massey 2005; Maxeiner et al. 2005; Lin et al. 2005; Kántor et al. 2016a) and also serve the correlation of ganglion cell activity (Hidaka et al. 2004; Schubert et al. 2005a, b; Völgyi et al. 2005, 2009, 2013a, b; Pan et al. 2010). As for the human retina, Cx36 and Cx45 have been reported to display expression patterns that resemble those of other mammalian species including the mouse, rabbit and rat (Feigenspan et al. 2001; Mills et al. 2001; Deans et al. 2002; Kihara et al. 2006, 2010; Söhl et al. 2010; Kovács-Öller et al. 2014). However, due to long postmortem time, the available partially decomposed human tissue rarely allows for a detailed observation of neuronal GJs. It has been shown that BCs form homologous and/or heterologous electrotonic coupling in the vertebrate retina, including primates (Marc et al. 1988; Mills 1999; Luo et al. 1999; Dacey et al. 2000). In contrast it is unknown if BC connections are established by the same designing rules in the human retina.

Multiple label immunohistochemistry experiments were performed to characterize Cx36 expressing BC interneurons of the human inner retina. Cx36 plaques were scattered throughout the entire inner plexiform layer (IPL). Several neurons and neuronal contacts were identified in which Cx36 comprises GJs, including the well studied AII–AII, AII-ON cone BC electrical synapses. In addition to these canonical GJ sites, putative homologous BC-to-BC Cx36 GJs were identified between neighboring diffuse bipolar type 3 and flat midget BCs and perhaps between diffuse bipolar type 6 cells as well. Other yet unidentified cellular contacts were also found, including putative GJs at AII ACs/diffuse type 3 physical contacts, GJs on AII primary dendrites, or Cx36 GJs that likely serve as signal conduits between parallel signaling streams. One such well represented example that was presented for the first time in this study is the formation of Cx36 GJs that connect midget pathway BCs to blue cone pathway giant bistratified bipolar cells. These findings suggest that regardless the signaling stream BC GJs serve both an intra-pathway correlation and an inter-pathway exchange of signals in the human retina prior integration by projectory ganglion cells.

Materials and methods

Human patients

Human donor tissue from patients ($n=4$, age: 37–64 years, 3 females, 1 male, postmortem time: 2.5–4 h) without reported history of eye disease was collected following the removal of corneas for transplantation in accordance with the tenets of Declaration of Helsinki. All personal identifiers were removed and samples were coded before histological processing. All experimental protocols were approved by the local ethics committees (TUKEB 58/2006, TUKEB 58/2014).

Histological preparation

After the removal of the corneas, posterior eyecups were fixed in 4% buffered paraformaldehyde for 2 h at +4 °C, cut in six radial slices then rinsed several times in 0.1 M phosphate buffered saline (PBS, pH 7.4). For whole mounts, the neural retina was carefully isolated from the mediotemporal parafoveal and peripheral area of the eye ball and the pigment epithelium was gently removed. The tissue was cut in small pieces, soaked overnight in 30% sucrose in PBS at +4 °C and stored in cryoprotectant solution for further use at −20 °C. For sections, inferonasal retinal pieces from the eyeball were placed into 30% sucrose in PBS at +4 °C then embedded in Thermo Scientific OCT (Life Technologies Hungary Ltd., Budapest, Hungary). Blocks were stored at −80 °C until sectioning. Ten to 20 µm sections were cut in the radial plane on a cryostat (Leica CM 1950, Leica Microsysteme, Wetzlar, Germany), sections were mounted on gelatin coated slides and stored at −20 °C until processing.

Fluorescent immunohistochemistry

Fluorescent immunohistochemical reactions on sections and on whole mounts were carried out according to standard protocols (Kántor et al. 2016a, b). To enhance penetration in the whole mounts, tissue was digested with 1% pepsin solution for 15 min at 37 °C and increased rinsing and incubation times were applied. Briefly, sections or tissue were washed several times with PBS (25 mM with 0.2% Triton-X, PBS-TX). Nonspecific background staining was blocked in 10% donkey serum diluted in PBS-TX. Specimens were then incubated in the primary antibodies at +4 °C (60 h for sections and 72 h for whole mounts).

Primary antibodies used in the present work are listed in Table 1. After extensive rinsing, specimens were incubated with the appropriate mixture of the following secondary antibodies: donkey anti-mouse IgG conjugated with Alexa 488 or DyLight 649 or Alexa 647 donkey anti-rabbit IgG conjugated with Alexa 488 or 555, donkey anti-guinea pig IgG conjugated to Rhodamine Red-X (Jackson ImmunoResearch Europe Ltd., Suffolk, UK) donkey anti-goat IgG conjugated with Alexa 555 (all Alexa conjugated antibodies were purchased from Life Technologies, Budapest, Hungary, all DyLight conjugated antibodies from Jackson ImmunoResearch Europe Ltd., Suffolk, UK) diluted in PBS-TX and 3% normal donkey serum. Staining with goat-PKCα was visualized using biotinylated horse anti-goat IgG (2 h, room temperature; Vector Laboratories, Enzo Life Sciences Ltd., Lörrach, Germany) and subsequent incubation with streptavidin conjugated to Pacific Blue (3 h, room temperature; Life Technologies, Budapest, Hungary). Sections were incubated for 3 h at room temperature, whole mounts overnight, at +4 °C. After several rinsing steps, whole mounts were mounted on gelatine coated slides and all specimens were coverslipped using AquaPolymount (Polysciences Europe GmbH, Eppelheim, Germany) as mounting medium. Slides were kept at +4 °C until imaging.

In cases when utilized primary antibodies were raised in the same species (e.g. anti-connexin36 and anti-protein kinase C alpha (PKCα) were both raised in mouse) fluorescent tyramide signal amplification (TSA) was carried out according to Hunyady et al. (1996). Briefly, first we carefully titrated the dilution of the first primary antibody (anti-PKCα) to determine the dilution where conventional immunostaining resulted in no detectable signal. Then we used the first primary antibody in this dilution (50-times more diluted than used for conventional immunohistochemistry) with biotin-TSA. After washing, sections were incubated with biotinylated goat anti-mouse IgG for 1 h at room temperature (1:500; Vector Laboratories, Burlingame, CA). After extensive rinses, TSA was carried out using a TSA Kit (Life Technologies Hungary Ltd, Budapest, Hungary) according to the manufacturer's manual and using Cy5 conjugated streptavidin as fluorophore (1:300, 3 h incubation; Jackson Immunoresearch Laboratories Inc., West Grove, PA, USA). Subsequently, conventional fluorescent immunohistochemistry (anti-Cx36) was applied on the sections.

Table 1 Primary antibodies used in this study

Antibody	Source	Host	Concentration	References
Mouse anti-connexin 35/36 (Cx36) clone 8F6.2	Merck Ltd., Budapest, Hungary	Mouse (monoclonal)	1:1000	Kántor et al. (2016a), O`Brien et al. (2012) and Kovács-Öller et al. (2014)
Rabbit anti-calretinin (CaR)	SWANT, Marly, Switzerland	Rabbit (polyclonal)	1:3000 in sections, 1:1000 in whole-mounts	Kántor et al. (2015, 2016a, b), Lee et al. (2016) and Eliasieh et al. (2007)
Goat anti-CaR	Merck Ltd., Budapest, Hungary	Goat (polyclonal)	1:3000	Puthussery et al. (2010)
Guinea pig anti-CaR	Synaptic Systems, Göttingen, Germany	Guinea pig (polyclonal)	1: 3000	Toader et al. (2013) and Tomassy et al. (2014)
Rabbit anti-calbindin D28k (CaB)	SWANT, Marly, Switzerland	Rabbit (polyclonal)	1:10,000 in sections, 1:1000 in whole-mounts	Kántor et al. (2016a, b), Eliasieh et al. (2007) and Weltzien et al. (2014)
Rabbit anti-recoverin (Rec)	Generous gift of Karl-Wilhelm Koch	Rabbit (polyclonal)	1:2000 insections, 1:1000 in whole mounts	Kántor et al. (2016a, b)
Rabbit anti-parvalbumin (PV)	SWANT, Marly, Switzerland	Rabbit (polyclonal)	1:10,000 in sections, 1:1000 in whole-mounts	Kántor et al. (2016a, b)
goat anti-parvalbumin (PV)	SWANT, Marly, Switzerland	Goat (polyclonal)	1:2000 insections, 1:1000 in whole mounts	Kántor et al. (2016a, b)
Mouse anti-protein kinase C alpha subunit (PKCα)	Santa Cruz Biotechniology Inc., Santa Cruz, CA, USA	Mouse (monoclonal)	1:50,000 for BTA	Kántor et al. (2016a, b)
Goat anti- PKCα	Santa Cruz Biotechniology Inc., Santa Cruz, CA, USA	Goat (polyclonal)	1: 1000	Chen et al. (2014)
Rabbit anti-RIBEYE A-domain	Synaptic systems, Göttingen, Germany	Rabbit (polyclonal)	1: 500	Regus-Leidig et al. (2010, 2014)

Imaging, image processing

Images were captured on a confocal microscope (Zeiss LSM 510 Meta or 780 with upright microscope Axio Imager Z1, Carl Zeiss Inc., Jena, Germany) or Leica TCS SP8, Leica (Microsystems Ltd., Wetzlar, Germany) using the ZEN 2012 (Carl Zeiss Inc., Jena, Germany) or Leica Application Suite X (Leica Microsystems Ltd., Wetzlar, Germany) software and 40× or 63× Plan-Apochromat oil-immersion lens (NA: 1.4). In the case of PKCα-RIBEYE-CaR-Cx36 quadruple fluorescent immunohistochemical reaction image deconvolution was carried out with the Huygens Essential Software (Scientific Volume Imaging B. V., Hilversum, The Netherlands), using classical deconvolution methods. Final images were constructed using Adobe Photoshop 7.0 (San Diego, CA, USA), Imaris 8.3 (Bitplane, Zürich, Switzerland) and Fiji (Schindelin et al. 2012). Only minor adjustments of brightness and contrast were applied, which in no case altered the original appearance of the images. Unsharp mask filter was only utilized in a few cases to avoid disturbing pixellation of images.

Colocalization analysis

To detect putative colocalization of Cx36 with other labeled (CaR, CaB, PV, PKCα, Rec) structures raw data were analyzed using the ZEN 2012 software (Carl Zeiss Microscopy, Jena, Germany). Fifty Cx36 plaques per stack from the proximal and distal half of the IPL were randomly chosen for analysis. Colocalization was suggestive if the maximal staining intensity of the Cx36 dot appeared in the same focal plane (Z dimension) as the maximal intensity of the second marker and no black pixels were detected between the two labeled structures. Orthogonal views of the stacks were generated and putative colocalizing sites were verified by measurements of the staining intensities. Histograms of staining intensities were generated along the *Z* axis. Colocalization of stainings was declared if the peaks of the histograms were found to be less than 9 pixels apart (750 nm, corresponding to the axial resolution limit of the confocal microscope). Note that orthogonal views were rescaled by ZEN to avoid image distorsion; thus the original Z voxel component (250 nm) was reduced to 84 nm to match the dimensions of the *X*–*Y* components. Areas covered by immunostained elements were determined using Fiji. To give a quantitative measure of colocalisations that is independent of marker frequency we weighed the number of colocalisations with the coverage factor of the corresponding neuronal marker.

Weighed colocalizations were calculated by utilizing a simple equation:

$$C_w = (C_p/A_p)/r_c,$$

where C_w is the weighed colocalization, C_p is the number of colocalized plaques, A_p is the number of analyzed plaques and r_c is the mean coverage ratio.

First, examined region of interest (ROI) areas were selected randomly in retinal samples. Coverage ratios (r_c) were then determined by dividing the area covered by the marker with the total area of the ROI. Cx36 plaques (A_p) were counted in each ROI and the number of real colocalisations (C_p) with the corresponding markers were determined (see above). Finally, the weighed colocalizations (C_w) for examined neuronal markers were calculated.

As control for chance colocalisation we performed flip control analyses. The analysis was performed on subsets of image stacks taken from Cx36-CaB-CaR (at the level of lobular appendages and transversal processes of AII amacrines) and Cx36-Rec (superficial part of IPL) labeled whole mounts. Cx36 plaques ($n=421$ at the level of lobular appendages, $n=219$ at the level of transversal processes in Cx36-CaB-CaR stained material and $n=855$ in the Cx36-Rec stained whole mounts) were manually marked using Neurolucida (Version 9, MBF Bioscience Europe, Magdeburg, Germany). Colocalization of Cx36 plaques with CaR and CaB alone, with CaR–CaB double stained processes or with Rec stained axons was noted. The analyzed volume measured 40×40×4 µm at the level of the lobular appendages, 15×15×3 µm at the level of the transversal processes in the Cx36-CaB-CaR stained material and 40×40×4 µm in case of the Cx36-Rec stained whole mounts. As control for chance colocalization, analysis was repeated on the same subsets of stacks after rotation of the Cx36 channel at 90°.

Neurolucida reconstruction

Cell bodies and axonal branches of flat midget, giant bistratified and diffuse type 3 BCs were manually traced using Neurolucida (Version 9, MBF Bioscience Europe, Magdeburg, Germany). Colocalizing Cx36 plaques and contact sites with outher stained neural elements were also marked. AII ACs were traced in a compartment specific manner. Cell bodies ($n=11$) and primary dendrites ($n=38$) were traced manually. Lobular appendages ($n=271$) with close appositions and transversal dendrites ($n=47$) in the deep ON sublamina were marked in 40×40×4 µm subsets of confocal Z stacks. Tracing of diffuse type 6 BC axons in the deep ON sublamina was not possible due to the dense CaB + fiber meshwork.

Results

Cx36 expression in the human retina

First, single labeling immunohistochemistry was carried out to detect Cx36 GJ sites in the human retina. The

utilized monoclonal antibody has widely been used to recognize Cx36 GJs in the nervous tissue of various mammalian models including humans and macaque (Kántor et al. 2016a, b; O'Brien et al. 2012; Rash et al. 2012; Kovács-Öller et al. 2014; Pereda et al. 2003). Similar to other mammalian species, the antibody recognized many Cx36 GJ plaques in both plexiform layers (Online Resource 1) in the human retina. Cx36 puncta were found throughout the entire IPL with the highest density in strata 4 and 5. A second discontinuous Cx36 rich area in strata 1–2 of the OFF sublamina was also evident, whereas the mid-IPL (stratum 3) appeared to show a Cx36 exclusion zone with lower magnification. However, a thorough examination of higher magnification images revealed the presence of a number of very faint and small Cx36 plaques in this area as well (Online Resource 1 inset). In this study, multiple-label immunohistochemistry experiments were carried out to mark selected BCs subtypes of the human retina and examine their Cx36 expression in the IPL (Cx36 expression in the OPL has been reported by Kántor et al. 2016b). The selection of criteria was to label BC subtypes serving each major parallel pathways. In this scheme parvocellular pathway signaling flat midget BC was stained for a recoverin (Rec; Haverkamp et al. 2003; Kántor et al. 2016a) antiserum, whereas the calbindin D28 (CaB) antiserum stained magnocellular pathway diffuse type3 BC (Luo et al. 1999; Jacoby et al. 2000; Grünert et al. 1994; Haverkamp et al. 2003; Percival et al. 2013; Masri et al. 2016) and koniocellular pathway signaling diffuse BC type 6 (Grünert et al. 1994; Haverkamp et al. 2003; Percival et al. 2011, 2013, 2014). In addition, a parvalbumin antiserum (PV) was utilized to stain giant bistratified BCs (Kolb et al. 1992; Kántor et al. 2016b), whose function has yet to be determined, as well as protein kinase C alpha (PKC_{α}; Haverkamp et al. 2003; Kántor et al. 2016a, b) that selectively stains rod BCs (RB) and to a lesser extent diffuse BC type 4 (Haverkamp et al. 2003). Finally, calretinin (CaR) was also utilized to distinguish between the numerous CaR/CaB dually stained AII amacrine cell (AC) processes and solely CaB + diffuse type 3 and diffuse type 6 BC axons (Lee et al. 2016; Kántor et al. 2016a, b). In addition to the above BC types, AII cells that appeared CaR/CaB double labeled in our specimen were also studied as they are constituent elements of the rod transversal signaling stream.

Flip controls were performed for labels CaR/CaB/Cx36 triple and Rec/Cx36 dual labeled whole mounts. These two samples were selected because they either possessed abundant labels for both Cx36 plaques and stained neuronal processes (CaR/CaB/Cx36) or contained sparse neuronal labeling (Rec/Cx36). Colocalizing and non-colocalizing plaque counts were performed for both original and flip control images and resulted percentages are provided in Online Resource 2. We found that flip controls display considerably less colocalizing (random) plaques even for the sparsely labeled Rec/Cx36 specimen than original images. These control experiments thus clearly show that colocalizations of Cx36 puncta in specified neuronal contacts are substantially higher than expected by mere chance.

To quantify Cx36 expression of neurochemically labeled profiles plaques were picked randomly in retinal cross-sections, true Cx36/marker colocalizations were determined (see methods) and then colocalization frequencies were calculated: (1) 90/167 (53%) CaR/Cx36 in the OFF and 108/200 (54%) in the ON sublaminas; (2) 79/226 (35%) and 152/250 (61%) CaB/Cx36 in the OFF and ON sublaminas; (3) 20/200 (10%) PV/Cx36 in the OFF and 21/200 (10.5%) in the ON sublamina; (4) 9/201 (4.5%) Rec/Cx36 in the OFF sublamina and (5) 26/204 (12%) PKC_{α}/Cx36 in the ON sublamina (Online Resource 3 and 4, Table 2). Since the above values greatly depends on the retinal coverage of each marker (e.g. CaR in the ON sublamina:0.34, and Rec in the OFF sublamina:0.04; see Table 2) weighed colocalization values were introduced (see "Materials and methods") to correct for differences in marker coverage (Online Resource 4c). This method revealed that probabilities for Cx36 colocalizations with CaR and CaB were high in both layers (ranging between 1.64 and 3.3) while they were modest for PV (0.77–0.8) and PKC_{α} (0.94). An unexpected finding was that contrary to the low coverage of Rec immunostained profiles the relative probability for Rec/Cx36 colocalizations was the highest (7.1). This suggested that although they were represented with a low frequency, the Rec + profiles in the OFF sublamina very often colocalized with Cx36 plaques.

Cx36 expression by diffuse BCs serving the magnocellular pathway

Besides the above analysis a thorough examination was carried out to determine celltype specific Cx36 GJ expression by BCs.

Diffuse type 3 OFF BC

CaB is expressed by diffuse type 3 BC cells in the primate and human retina (Haverkamp et al. 2003; Kántor et al. 2016a, b). Our CaB labeled specimen confirmed this observation, however, the numerous AII cell profiles in all IPL layers greatly impeded the identification of diffuse type 3 BC axons in the CaB/Cx36 stained material (Fig. 1b). As human AII cells also express CaR (Fig. 1a; Lee et al. 2015; Kántor et al. 2016b), the CaR/CaB/Cx36 triple-stained material allowed for the discrimination of CaR/CaB dual labeled AII cell processes from the solely CaB + BC axon terminals in the OFF sublamina. Diffuse type 3 BC axons and AII lobular appendages often formed

Table 2 Colocalization frequency of Cx36 plaques with neuronal markers in the human retina

	Marker abs cov (μm^2)	Mean cov ratio (r_c)	SD	# of coloc puncta (C_p)	# of analyzed plaques (A_p)	Weighed coloc (C_w)
CaR str. 1–3 ($n=30$)	7036.6	0.23	0.06	90	167	2.3
stack1 ($n=6$)	1741	0.16	0.02	7	44	1.01
stack2 ($n=6$)	1160.3	0.24	0.02	3	18	0.68
stack3 ($n=6$)	1533.3	0.27	0.05	23	32	2.63
stack4 ($n=6$)	980.6	0.25	0.05	12	30	1.55
stack5 ($n=6$)	1621.2	0.23	0.04	25	43	2.6
CaR str. 4–5 ($n=24$)	4985.4	0.34	0.05	108	200	1.64
stack1 ($n=6$)	1663.4	0.29	0.03	16	50	1.1
stack2 ($n=6$)	903.1	0.32	0.03	19	50	1.18
stack3 ($n=6$)	1264.2	0.39	0.07	30	50	1.54
stack4 ($n=6$)	1154.7	0.35	0.02	43	50	2.45
CaB str. 1–3 ($n=30$)	4015.7	0.2	0.04	79	226	1.74
stack1 ($n=6$)	831.5	0.25	0.04	16	50	1.37
stack2 ($n=6$)	659.5	0.19	0.02	13	50	2.6
stack3 ($n=6$)	699.6	0.18	0.02	22	47	2.1
stack4 ($n=6$)	1029.9	0.22	0.03	19	41	1.55
stack5 ($n=6$)	801.2	0.18	0.02	24	50	2.66
CaB str. 4–5 ($n=30$)	3872.7	0.2	0.05	200	250	3.33
stack1 ($n=6$)	719.7	0.28	0.07	37	50	2.64
stack2 ($n=6$)	1131.8	0.29	0.02	42	50	2.9
stack3 ($n=6$)	801.8	0.23	0.03	39	50	3.4
stack4 ($n=6$)	475.6	0.19	0.01	37	50	3.9
stack5 ($n=6$)	743.8	0.21	0.02	45	50	4.3
PV str. 1–3 ($n=19$)	2313.5	0.13	0.06	20	200	0.77
stack1 ($n=6$)	490	0.11	0.01	1	50	0.18
stack2 ($n=3$)	547.7	0.19	0.06	11	50	1.15
stack3 ($n=5$)	732.1	0.18	0.05	4	50	0.44
stack4 ($n=5$)	543.8	0.11	0.01	4	50	0.72
PV str. 4–5 ($n=18$)	1620.7	0.14	0.09	21	200	0.8
stack1 ($n=6$)	165.6	0.04	0.02	10	50	5
stack2 ($n=3$)	528.1	0.23	0.02	3	50	0.26
stack3 ($n=3$)	611.1	0.27	0.02	1	50	0.07
stack4 ($n=6$)	315.9	0.11	0.01	7	50	1.27
PKC_α str. 4–5 ($n=24$)	3422.6	0.15	0.02	26	198	0.94
stack1 ($n=6$)	503.3	0.14	0.01	13	50	1.86
stack2 ($n=6$)	729.3	0.13	0/03	3	50	0.46
stack3 ($n=6$)	664.5	0.16	0.01	6	48	0.78
stack4 ($n=6$)	1525.5	0.16	0.02	4	50	0.5
Rec str. 1–3 ($n=24$)	1125.9	0.04	0.02	57	200	7.125
stack1 ($n=6$)	280.1	0.04	0.01	9	50	4.5
stack2 ($n=6$)	330.1	0.04	0.01	24	50	12
stack3 ($n=6$)	314.3	0.02	0.003	15	50	15
stack4 ($n=6$)	201.4	0.04	0.01	9	50	4.5

abs cov absolute coverage, *mean cov* mean coverage ratio (r_c; see methods), *SD* standard deviation, *coloc* colocalisation, *str* stratum, *CaR* calretinin, *CaB* calbindin, *PV* parvalbumin, *PKC_α* protein kinase C alpha subunit, *Rec* recoverin

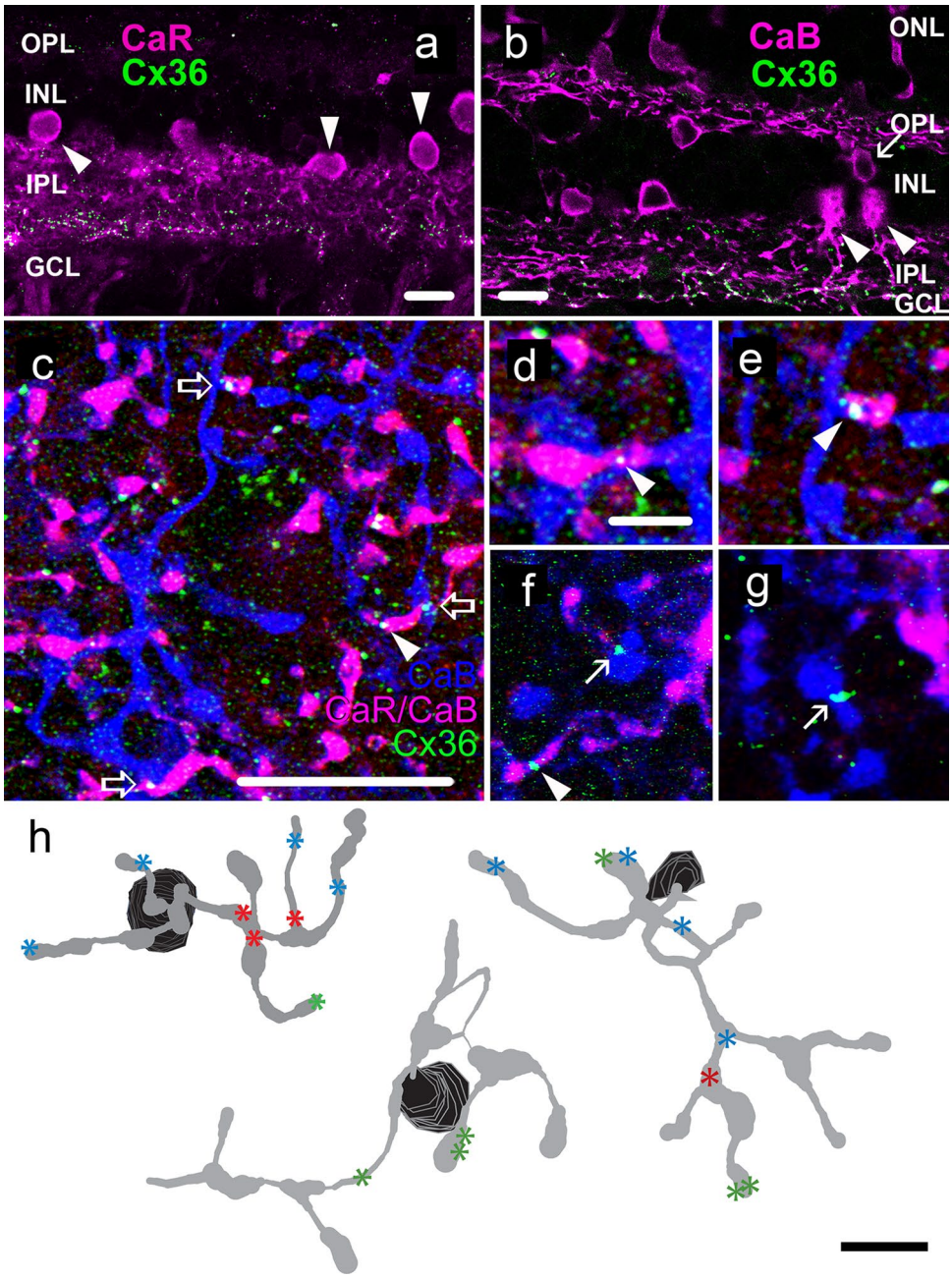

Fig. 1 Cx36 plaque expression by magnocellular pathway diffuse type 3 BC cell axonal processes. **a** CaR immunolabeling (*magenta*) is displayed by a cohort of inner retinal cells, including AII ACs (*arrowheads*) in the human retina. Cx36 plaques (*green*) often colocalize with AII cell processes in the ON sublamina of the IPL. **b** CaB positivity (*magenta*) is exhibited by cones, horizontal cells, BCs (*arrow*) and AII ACs (*arrowheads*) in the human retina. Similar to CaR labels, CaB stained AII dendrites bear many Cx36 plaques. **c** Photomicrograph focusing on the OFF sublamina of a whole mount human retina specimen. The image displays Cx36 plaques (*green*), AII AC lobular appendages that express both CaR (*red*) and CaB (*blue*), thus appearing (*magenta*), as well as purely CaB labeled diffuse type 3 BC (DB3) axons and axon terminals (*blue*) in the OFF sublamina. Cx36 plaques occur at AII–AII (*arrowheads*) and AII-diffuse type 3 BC (*open arrows*) interfaces. **d**–**g** Higher magnification images display close association of AII lobular appendage pairs (*arrowheads*) and diffuse type 3 BC axonal endings (*arrows*), some of which displays Cx36 plaques. **h** Neurolucida reconstructions display somata (*black*) and axon terminals (*gray*) of reconstructed diffuse type 3 BCs as well as colocalizing Cx36 plaques (*asterisks*). Colocalizing Cx36 plaques were found in diffuse type 3 BC-diffuse type 3 BC axonal crossings (*green asterisks*), diffuse type 3 BC-AII process crossings (*blue asterisks*) or in diffuse type 3 BC axonal processes without any stained contact partner (*red asterisks*). *ONL* outer nuclear layer, *OPL* outer plexiform layer, *INL* inner nuclear layer, *IPL* inner plexiform layer, *GCL* ganglion cells layer. *Scale bars* **a**–**c** and **h** 10 µm, **d**–**g** 2 µm

appositions that very likely represented locations of glycinerg synaptic inputs from AII cells to diffuse type 3 BC BCs (Fig. 1c–g). Despite the relative low number of Cx36 plaques in the OFF sublamina diffuse type 3 BC axons colocalized with Cx36 puncta frequently with 4.5 plaques in average in the axonal arbor (±2.7 SD, $n=8$ reconstructed diffuse type 3 BC axons; see Table 3). These colocalizing plaques could be found throughout the diffuse type 3 BC arbor with a somewhat higher chance for 2nd–4th order mid-arbor axonal brances (Online Resources 3; Table 3). Moreover, some colocalizing Cx36 plaques (mean = 2 ± 1.8 SD, $n=8$ reconstructed axons) were located at interfaces of two neighbor diffuse type 3 BC axons (Fig. 1h). Such sites likely represented diffuse type 3 BC-to-diffuse type 3 BC GJs. Curiously, Cx36 plaques quite often (11–27 in each selected 40 × 40 µm area in $n=4$ stacks; see Table 2 and text on AII ACs) were found at sites of AII AC and diffuse type 3 BC axon contacts. This finding suggests that the signaling between these two interneurons is more complex than it has previously been thought and besides the known glycinerg inhibition, AII ACs and diffuse type 3 BC cells may maintain GJ contacts as well.

Cx36 expression by midget BCs serving the parvocellular pathway

Flat midget OFF BC

The Rec serum utilized in this work specifically stained flat midget BCs (Haverkamp et al. 2003; Kántor et al. 2016a, b), whose axonal processes arborized in stratum 2 (Fig. 2a). A thorough analysis of the Rec/Cx36 double labeled specimen was carried out to find colocalizations between flat midget BC axons and Cx36 plaques. As it has been pointed out above the absolute number of such colocalizations were rather low (9 out of 201 examined plaques is 4.5%) but due to the low Rec coverage the relative colocalization frequency was the highest for Rec/Cx36 in or specimen (Online Resource 3 and Table 2). The selective Rec labeling allowed for detailed morphological examination of flat midget BCs. Six flat midget BC cells were selected for Neurolucida reconstruction and subsequent morphometric analysis (details regarding flat midget BC cells are shown in Table 3). The morphometric data reveals that reconstructed flat midget BC axons possessed 15–19 (mean = 17.5 ± 1.38 SD) colocalizing Cx36 plaques. Although colocalizing plaques could be found throughout the axonal arbor (1–8th axonal order) but they were most frequent on higher order (4–7th order) axonal branches and terminal endings (Online Resources 3; Table 3). In addition, many colocalizing Cx36 puncta (79 out of 105; $n=6$ flat midget BCs) preferentially located at axonal sites in the vicinity of axonal varicosities or at axonal endings both are likely locations of chemical synapses (Table 3). Axonal crossings of neighbor flat midget BCs were thoroughly examined for colocalizing Cx36 plaques. Flat midget BC axonal arbors seemed to overlap little thus giving little chance for homologous axonal GJs. Although, such Cx36 colocalizations at axonal crossings were found in both whole mounts and sections but they appeared rare (Fig. 2). Out of the 105 colocalizing Cx36 plaques only one occurred at axonal crossings of reconstructed flat midget BCs (Table 3). Even though well isolated flat midget BCs were purposely selected for the better Neurolucida reconstruction, it is clear that the majority of colocalizing Cx36 plaques were not related to flat midget BC-to-flat midget BC axonal crossings. However, flat midget BC contacts with intervening Cx36 plaques were also found arguing for the presence of homologously coupled flat midget BC syncytium (Fig. 2h–i). This was further supported by the fact that besides mid-axon Cx36 also axon-tip plaques were seen (Table 3).

Cx36 expression by BCs serving the koniocellular pathway

Diffuse type 6 ON BC

In addition to diffuse type 3 BC BCs, the CaB serum labeled BCs whose axons terminated in the ON sublamina. These CaB + cells have been identified previously as diffuse type 6 ON BCs (Haverkamp et al. 2003; Jusuf et al. 2004; Kántor et al. 2016a, b). The CaR/CaB/Cx36 specimen again allowed for the distinction between CaB/CaR dually labeled AII transversal processes and CaB + diffuse type 6 axons in the ON sublamina. In this material Cx36 plaques often occured at crossings of AII cell transversal dendrites and diffuse type 6 axons (Fig. 3d) as a clear indication of AII-to-diffuse type 6 GJs. In addition to heterologous AII-to-diffuse type 6 GJs, Cx36 plaques were seen at BC-to-BC interfaces as well indicating the presence of homologous GJs among CaB + diffuse type 6 ON BCs (Fig. 3a–c). Finally, Cx36 plaques were found on diffuse type 6 axon processes without apparent contacting neuron. This suggested that diffuse type 6 cells may form GJs with other unlabeled (non-AII, non-diffuse type 6) retinal neurons.

Cx36 expression by BCs potentially serving the blue cone pathway

Giant bistratified ON–OFF BC

PV + BCs displayed the giant bistratified morphology (Kolb et al. 1992; Kántor et al. 2016b) that formed a relatively sparse BC population. The relative thick axons of giant bistratified BC cells first arborized in the OFF sublamina, where they gave off axonal branches extending several tens of

Table 3 Morphometric and Cx36 colocalization data of Neurolucida reconstructed flat midget BC, giant bistratified BC and diffuse type 3 BC in the human retina

	# of Cx36 coloc. ind. ax	# of Cx36 coloc. ax cross.	Cx36 axonal distribution	# of Cx36 plaques around varicosity	# of axonal nodes	max axonal order	# of axonal endings	Total axonal length (µm)
FMB(1)	17	1	0/0/1/3/5/7/2	10	11	7	12	172.9
FMB(2)	18	0	1/1/2/2/0/3/6/3	14	9	8	11	171.7
FMB(3)	18	0	0/3/3/3/5/2/1	15	11	7	12	172.5
FMB(4)	18	0	0/0/0/1/5/7/5	15	12	7	13	215.2
FMB(5)	19	0	0/0/7/0/3/6/1/3	14	8	8	9	165.5
FMB(6)	15	0	1/1/0/4/5/0	11	9	6	11	152.2
FMB mean	17.5 ± 1.4 SD	0.2 ± 0.4 SD		13.2 ± 2.1 SD	10 ± 1.5 SD	7.2 ± 0.7 SD	11.3 ± 1.4 SD	175.5 ± 21.2 SD
GBB(1)	17	0	0/2/2/11/0/0/2/0	NA	10	8	11	404.7
GBB(2)	6	0	0/1/0/0/3/6/1/0/0/1	NA	10	10	9	138.4
GBB(3)	7	0	5/0/2	NA	2	3	3	103.5
GBB(4)	14	0	0/1/1/0/1/4/1/4/2	NA	8	9	9	186.6
GBB(5)	1	0	0/0/0/0/1/0/0	NA	9	7	11	271
GBB(6)	6	0	0/0/0/0/4/2	NA	7	6	8	178.9
GBB(7)	2	0	0/2/0	NA	2	3	3	153
GBB(8)	2	0	0/1/1	NA	2	3	3	120.6
GBB(9)	12	0	0/1/4/6/1/0	NA	9	6	11	267.1
GBB(10)	7	0	0/3/3/1	NA	3	4	5	137.2
GBB(11)	2	0	0/0/1/1/0	NA	9	7	11	189.3
GBB mean	6.9 ± 13.8 SD	0		NA	6.45 ± 3.44 SD	6 ± 2.5 SD	7.64 ± 3.5 SD	195.5 ± 88 SD
	# of Cx36 coloc. ind ax	# of Cx36 coloc. ax cross	Cx36 axonal distribution	# AII lob-app/ DB3 contacts	# of axonal nodes	Max axonal order	# of axonal endings	Total axonal length (µm)
DB3(1)	3	1	0/1/2/0/0	12	4	5	5	67
DB3(2)	4	4	0/1/3/0/0	9	4	5	6	57.5
DB3(3)	6	5	0/2/0/1/0/0	8	5	6	6	66.2
DB3(4)	4	2	0/0/3/0/0	9	5	5	6	72.1
DB3(5)	0	0	0/0/0/0/0	5	4	5	6	50.4
DB3(6)	8	3	0/1/2/4	6	6	4	7	82.6
DB3(7)	8	1	0/2/2/2/3	9	5	5	6	80
DB3(8)	3	0	NA	3	NA	NA	NA	NA
DB3 mean	4.5 ± 2.7 SD	2 ± 1.8 SD		7.6 ± 2.8 SD	4.7 ± 0.8 SD	5 ± 0.6 SD	6 ± 0.6 SD	68 ± 11.5 SD

Column 3 with the label Cx36 'axonal distribution' provides the numbers of colocalizing Cx36 plaques located in 1st/2nd/3rd/...etc. axonal branches

coloc. colocalization, *ind*. individual, *ax*. axon, *cross*. crossing, *max*. maximum, *lob-app*. lobular appendages, *FMB* flat midget bipolar cell, *GBB* giant bistratified bipolar cell, *DB3* diffuse type 3 bipolar cell

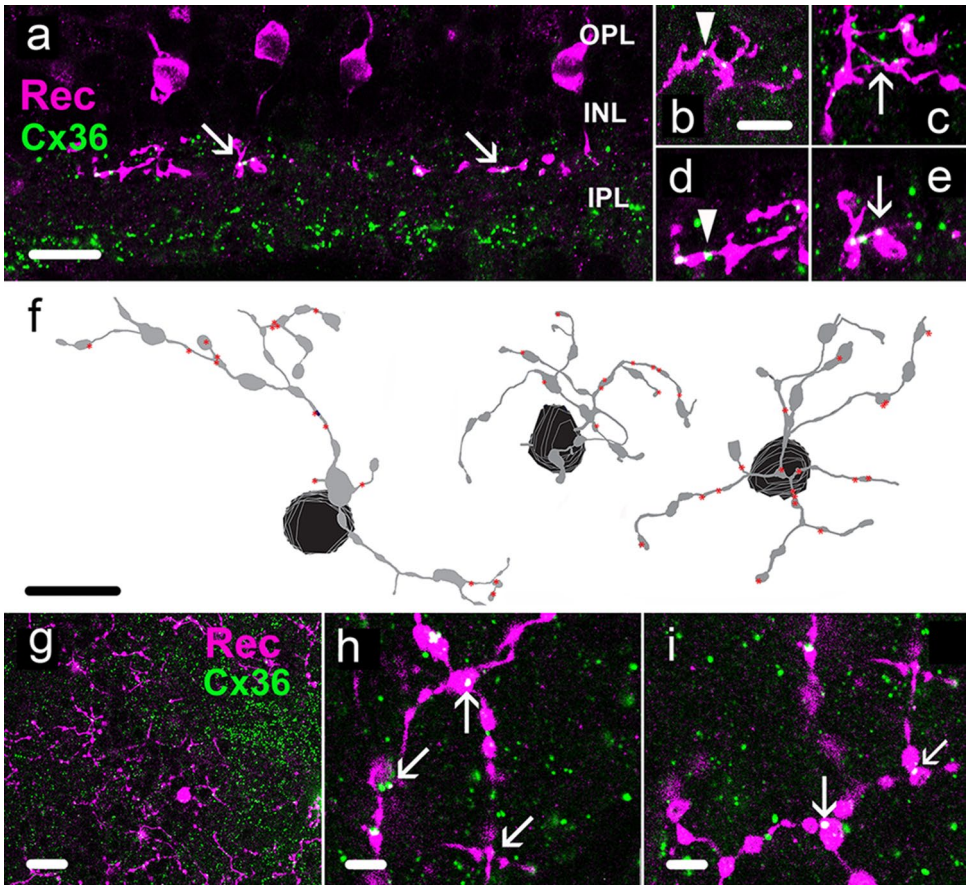

Fig. 2 Parvocellular flat midget BC cells express Cx36 plaques on their axonal processes. **a** Photomicrograph showing a retinal cross-section with Rec + flat midget BC cells (FMB; *magenta*) and Cx36 plaques (*green*). Plaques in the OFF sublamina often colocalized with flat midget BC axons (*arrows*). **b–e** Colocalizations occurred on sole flat midget BC axons without stained contact partner (*arrowhead*) as well as axon-to-axon contacts of flat midget BCs (*arrows*). **f** Neurolucida reconstructions display somata (*black*) and axon terminals (*gray*) of flat midget BCs. *Red asterisks* represent Cx36 plaques that were located throughout the axonal arbor of flat midget BC cells. **g–i** Whole mount human retina specimen displays Rec + flat midget BC axons (*magenta*) and Cx36 plaques (*green*). Occasionally, Cx36 plaques are located at axonal contacts of neighboring flat midget BCs (*arrows*). *OPL* outer plexiform layer, *INL* inner nuclear layer, *IPL* inner plexiform layer. *Scale bars* **a, f, g** 10 µm, **b–e, h** and **i** 2 µm

micrometers horizontally (Fig. 4a–d). In addition, many giant bistratified BC axonal branches reached the mid-IPL or even deep ON IPL areas and stretched horizontally similar to their counterparts in the OFF sublamina. Neurolucida reconstructions and subsequent morphometric analysis were performed to obtain an overview on giant bistratified BC cell morphology (see Table 3; Fig. 4d). Giant bistratified BCs displayed Cx36 plaques on their axons but the number of these colocalizing plaques varied in a wide range (1–17; mean = 6.9 ± 13.8 SD). Plaques could be located anywhere along the giant bistratified BC axonal tree with a slight preference for the middle portion of the axons (Online Resources 3; Table 3). Similar to flat midget BC cells the sparsity of giant bistratified BCs and the loose retinal coverage of their axons offered relatively little chance for overlaps of neighbor axonal branches. In some occasions giant bistratified BC axonal overlaps were present (Fig. 4), however, none of the $n = 11$ reconstructed giant bistratified BCs displayed Cx36 plaques at axonal crossings (Table 3). This suggested that if giant bistratified BC-to-giant bistratified BC homologous GJs exist they are very scarce. In the PV/CaB/Cx36 material giant bistratified BC axonal processes displayed close appositions with putative AII lobular dendrites indicating glycinerg inhibitory inputs from AII cells to giant bistratified BCs (Fig. 4e–h). Interestingly, Cx36 plaques were evident in a few of these close giant bistratified BC/putative AII physical contacts.

Cx36 expression by human interneurons of the rod signaling pathway

Rod BC (RB)

Contrary to the numerous Cx36 plaques and large PKC_{α} stained RB axonal profiles in the ON sublamina only

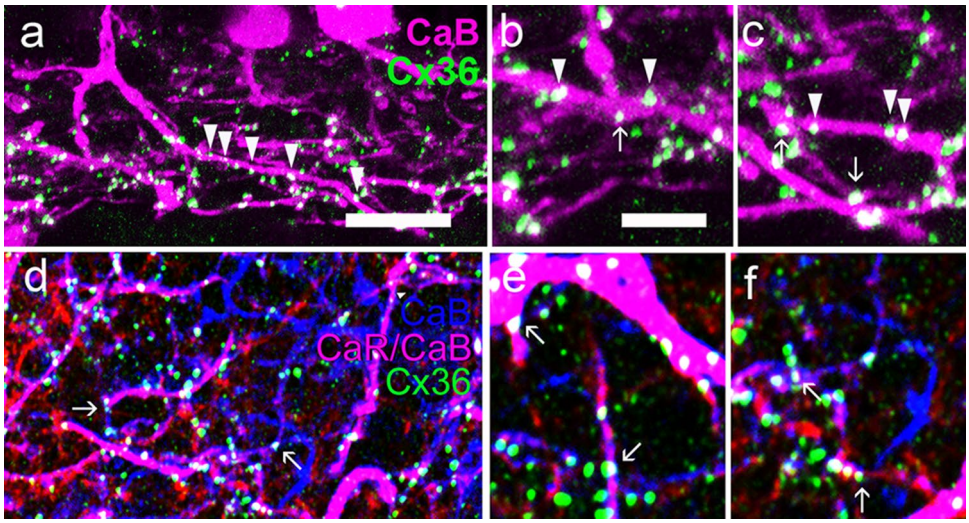

Fig. 3 Koniocellular pathway diffuse type 6 BCs express Cx36 GJs. **a-c** Cross-sections of the inner retina display CaB + diffuse type 6 BC axons (*magenta*) and Cx36 plaques (*green*). Many immunolabeled Cx36 plaques colocalized with the axon of diffuse type 6 BCs (**a**; *arrowheads*). Such colocalizations were even more obvious in the higher magnification images (**b, c**). Some of these colocalisations occurred at crossings of neighbor diffuse type 6 BC axons (*arrow*). **d–f** Retinal whole mounts display CaR (*red*) and CaB (*blue*) dually stained AII transversal dendrites (*magenta*), CaB + diffuse type 6 BC axons (DB6; *blue*) and Cx36 plaques (*green*). Crossings of AII dendrites and diffuse type 6 axons often display Cx36 plaques (*arrows*) that can be clearly resolved in the high magnification images (**e, f**). *Scale bars* **a, d** 10 µm, **b, c, e, f** 2 µm

26 out of 198 Cx36 plaques (13%) appeared to colocalize with RB processes (Fig. 5) and the calculated PKC_{α}/Cx36 weighed colocalization was rather low (0.94; Table 2). Any colocalization, however, was unexpected, as RBs are well known for the lack of coupling in previously examined mammals. A few, but not all, colocalizations could be accounted for DB4 cone BCs that have also been reported to express PKC_{α} (Haverkamp et al. 2003). To elucidate if the corresponding Cx36 plaques rather belonged to juxtapositioned AII ACs, however, triple labeling experiments were carried out for PKC_{α}/CaR/Cx36. In this specimen, the majority of apparent PKC_{α}/Cx36 colocalizations were juxtaposed to CaR + AII transversal dendrites or CaR + AII cell dendritic crossings (Fig. 5b–e). This observation thus attested that the apparent PKC_{α}/Cx36 colocalizations were in fact sites of AII-to-AII and/or AII-to-cone BC GJs that were juxtaposed to RB axon terminals. The frequent proximality of RB axon profiles to AII GJs further suggested a strategical vicinity of glutamatergic RB inputs to AII cell GJs. To test this, quadruple labels were performed to stain ribbon synapses with RIBEYE, Cx36 and processes of both PKC_{α} labeled RBs and CaR + AII cells. In fact, this experiment showed that many AII Cx36 plaques were in juxtaposition with RB ribbon synapses (Fig. 5f–j) thus supporting the above hypothesis.

AII ACs

AII cells are essential interneurons in vertical signaling via the so called primary rod pathway. AII ACs also express Cx36 to form GJs with neighbor AII cells and ON cone BCs (Deans et al. 2002). AII cells could be best examined in the CaR/CaB labeled material of this study where most dually stained somata and dendrites belonged to AII cells. Single labeled structures on the other hand were non-AII ACs, BCs or GCs. In human retinal samples of this study AII cells appeared to show the most numerous colocalizations with Cx36 plaques (Fig. 6a, b). AII cells are highly compartmentalized neurons thus their Cx36 expression was examined in a compartment specific manner. Most Cx36 colocalizations, as expected were found on AII cell transversal dendrites in the ON sublamina (Fig. 6a, b). To quantify this, 40 × 40 µm areas ($n = 4$ from different samples; see Table 4) were selected and some transversal branches were traced for Cx36 plaques. 10–14 individual transversal branches/ROI were analyzed (mean = 11.7 ± 1.7 SD) that added up to of 320–420 µm (mean = 374.2 ± 46.4 SD) AII transversal processes. Each selected area contained 106–164 colocalizing Cx36 plaques (mean = 132.5 ± 24.2 SD) with remarkably high plaque density (0.38–0.53 plaque/µm dendrite, mean = 0.49 ± 0.07 SD). Approximately one third of

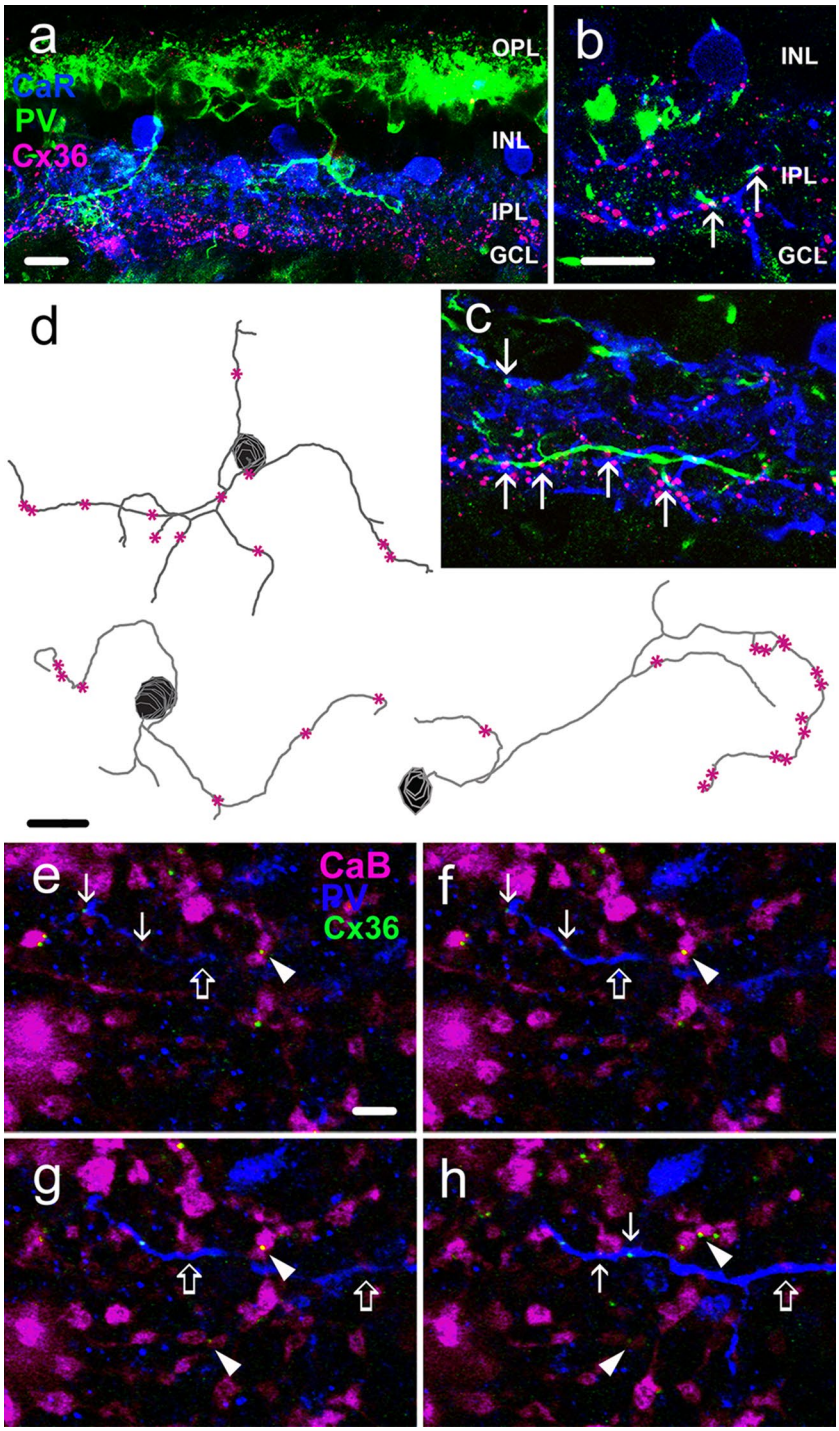

Fig. 4 Cx36 punctate labels overlap with putative blue cone pathway giant bistratified BC cell axons in the IPL. **a** Retinal cross-section shows PV + giant bistratified BC cells (*green*) with complex axonal branching pattern, CaR + AII cells (*blue*) and Cx36 immunolabeled plaques (*magenta*). Giant bistratified BC axons were found throughout the IPL with a quasi bistratification in the ON and OFF sublaminae. **b, c** High magnification images show that Cx36 plaques in the IPL often overlap and colocalize with giant bistratified BC axonal processes (*arrows*). **d** Neurolucida drawings exhibit the loose branching pattern of giant bistratified BC axons and the occasional colocalization of Cx36 plaques (*red asterisks*). **e–h** Image series displays four consecutive frames of a PV + giant bistratified BC (GBB) axon branch (*blue*) and CaB + AII cell profiles (*magenta*) in the OFF sublamina. Putative homologous AII–AII contacts with colocalizing Cx36 puncta (*arrowheads*) are often observed. AII to giant bistratified BC physical contacts (*open arrows*) and giant bistratified BC-Cx36 colocalizations (*arrows*) are less frequent. *OPL* outer plexiform layer, *INL* inner nuclear layer, *IPL* inner plexiform layer, *GCL* ganglion cells layer. *Scale bars* **a, d** 10 µm, **b, c, e–h** 2 µm

colocalizing Cx36 puncta (41–58; mean = 47.5 ± 7.6 SD) were located at crossings of two AII transversal processes indicating the high density of AII–AII GJs (Fig. 6j). Although, AII lobular appendages in the OFF sublamina are not classical sites for AII GJs but they clearly maintained Cx36 plaques in human samples of this work (Fig. 6g–i). 40 × 40 µm areas ($n = 4$ from different samples) were selected for Cx36 plaque count, in which all lobular appendages were examined (Table 4). In each of the selected areas 3–5 lobular dendrites (mean = 4 ± 0.7 SD) displayed contacts bearing Cx36 plaques with other appendages, 35–52 (mean = 47.5 ± 8.3 SD) with CaB + diffuse type 3 BC axon fibers, 0–5 with putative CaR + ACs or GCs (mean = 1.7 ± 2.2 SD) and remained solitary in a few cases (10–15; mean = 12.75 ± 2.1 SD). Out of these numerous AII contacts in the OFF

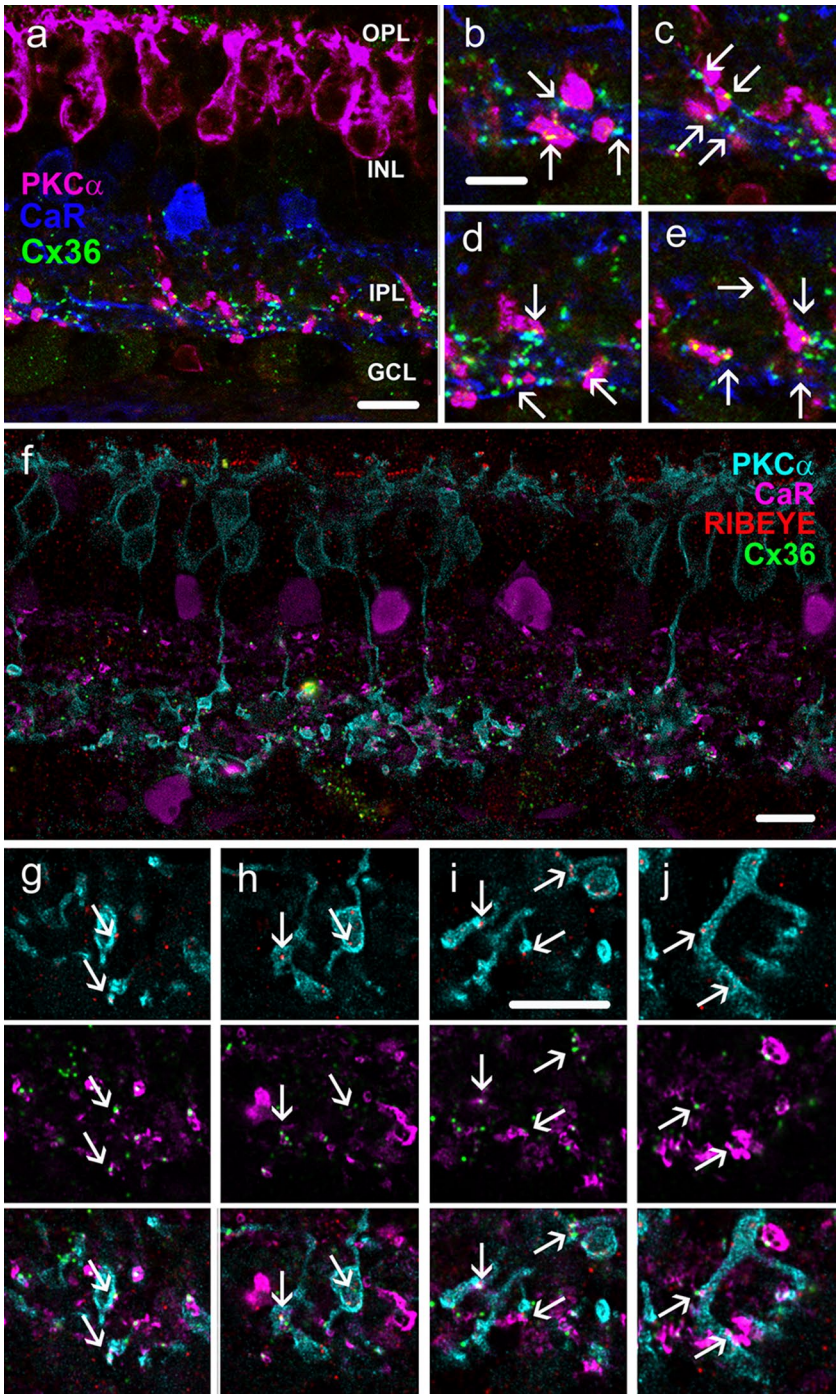

Fig. 5 Cx36 punctate labels overlap with PKC_{α} labeled rod bipolar cell (RB) axonal processes. **a–e** Retinal cross sections display results of a PKC_{α} (*magenta*), CaR (*blue*) and Cx36 (*green*) triple labels. RB axons often form close associations with putative postsynaptic AII AC transversal dendrites at sites where AII cells form Cx36 GJs (*arrows*). **f–j** Quadruple labels display PKC_{α} labeled RB cells (*turquoise*), CaR stained AII cells (*magenta*), Cx36 plaques (*green*) and presynaptic ribbon marker RIBEYE plaques (*red*). The retinal crossection (**f**) exhibits many sites where RB axons are in juxtaposition with AII transversal dendrites. Higher magnification panels (**g–j**) display RIBEYE containing RB axons (*upper panels*) in a presynaptic position to AII transversal dendrites that harbor nearby Cx36 plaques (*middle panels*). Composit panels at the bottom exhibit many sites where presynaptic RB ribbons are in juxtaposition to Cx36 plaques of the postsynaptic AII dendrite (*arrows*). This suggests a strategic positioning of AII GJs in the vicinity of inputs from RB cells. *OPL* outer plexiform layer, *INL* inner nuclear layer, *IPL* inner plexiform layer, *GCL* ganglion cells layer. *Scale bars* **a, f, g–j** 10 µm, **b–e** 2 µm

sublamina, each examined area contained only few (3–5) AII lobular-to-lobular dendrite contact sites with clear Cx36 plaque colocalization (Fig. 6g–i). In contrast, AII dendrite/diffuse type 3 BC axon contact sites exhibited frequent (11–27) colocalizations with Cx36 plaques. An even more unexpected finding was that many (10 out of 11 partially reconstructed AII cells; Table 4) AII AC cell somata displayed one or more Cx36 plaques on their surface (Fig. 6c–f). In many cases one or more (up to 5) Cx36 plaques were observed at the soma base very close to the emerging primary dendritic trunk. In addition, the proximal primary dendrites in stratum 1 often (2–5/AII cell; $n = 11$ reconstructed AII cells) displayed Cx36 plaques as well. Whereas somatic Cx36 plaques did not always show evidence for a postsynaptic neuronal structure (except Cx36 plaques between neighboring AII somata), those located on proximal dendritic trunks displayed (5 out of 11; $n = 11$ reconstructed AIIs) putative

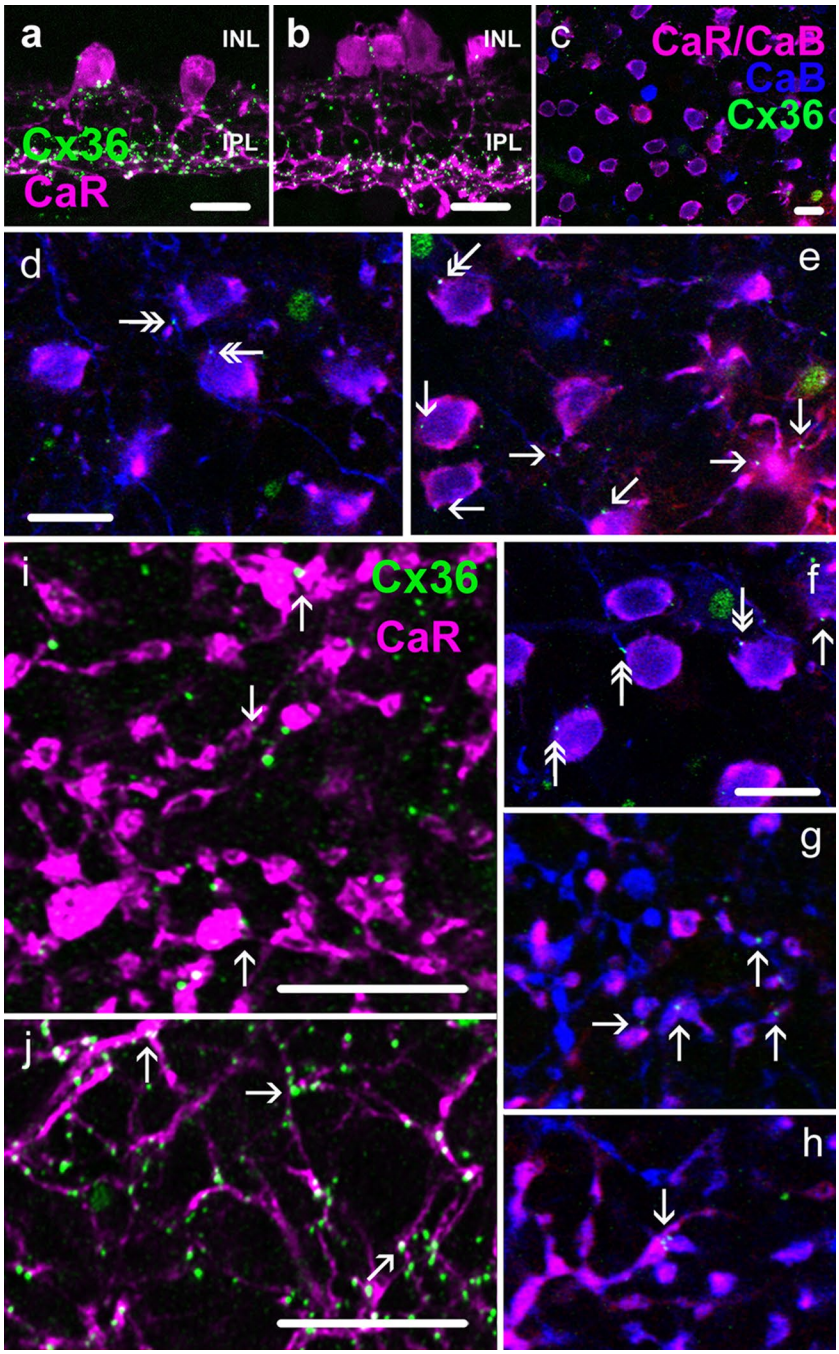

Fig. 6 Cx36 plaques are associated with various AII AC compartments. **a, b** Cross sections show that Cx36 puncta (*green*) colocalize with CaR + AII AC somata (*magenta*), lobular dendrites, primary dendritic trunks and transversal dendrites in the IPL. In some occasions somatic Cx36 plaques appeared to connect two neighboring AII cell bodies (**b**). **c–j** Whole mount specimen display a closer look at Cx36 (*green*) colocalizations with various CaR (*red*) and CaB (*blue*) double labeled AII AC compartments. When the plane of focus is set to the INL Cx36 puncta often appear on AII somata and/or the primary dendrites near to their somatic origin (*arrows*, **d–e**). In some cases these primary dendritic Cx36 plaques occur at sites where CaB + wide-field AC processes are in close physical vicinity (*double headed arrows* in **d–f**). In addition, AII AC lobular appendages appear to contact each other and such contact sites often display Cx36 puncta in CaR/CaB/Cx36 (**g, h**) and CaB/Cx36 (**i, j**) labeled specimen. **j** AII AC transversal dendrites display a number of colocalizing Cx36 puncta, many of which occur at AII dendritic crossings. *INL* inner nuclear layer, *IPL* inner plexiform layer. *Scale bars* 10 µm

postsynaptic structures. These latter profiles belonged to either CaR + or CaB + neurons that showed characteristics of wide-field ACs.

Cx36 plaques in heterologous BC contacts

It has been demonstrated that BCs of the vertebrate retina may form GJs with other retinal interneurons. While the AII-to-ON cone BC contacts remain the sole example for BC-to-AC GJs there is evidence that BCs can couple to BC neighbors via electrical synapses in both lower vertebrates and mammals (Marc et al. 1988; Mills 1999; Luo et al. 1999; Dacey et al. 2000). Besides the above examples for homologous (same type) BC GJs, the next section will provide examples for heterologous BC-to-BC GJs. The rationale to look for such heterologous junctions stems from the numerous observed Cx36 colocalizations with BC axons with no apparent same type synaptic partner.

Table 4 Morphometric and Cx36 colocalization data of reconstructed AII ACs in the human retina

	Cx36 pl. soma side/ app str.	Cx36 pl. soma base/ app str.	Cx36 pl. prox dt/ app str.	Soma surface (μm^2)	# of primary dendrites	
AII #1	1/0	5/0	1/0	195.8	4	
AII #2	2/0	3/0	2/2	178.3	2	
AII #3	2/0	0/0	4/3	220	4	
AII #4	1/0	1/0	0/0	268.1	5	
AII #5	0/0	0/0	0/0	198	3	
AII #6	3/0	2/0	8/0	212.4	4	
AII #7	1/0	1/0	2/0	213.9	3	
AII #8	0/0	2/0	3/1	235.2	3	
AII #9	1/0	1/0	2/0	202.2	4	
AII #10	1/0	0/0	4/1	185.2	2	
AII #11	0/0	1/0	2/1	201.3	4	
	AII lob-app/DB3 wo. plaque	AII lob-app/DB3 with 1 or 2 pl	AII lob-app/ no contact	AII lob-app/lob-app 1 or 2 pl	AII lob-app/CaR 1 pl	AII lob-app/ no contact 1 pl
Subset 1	32	20	13	4	1	1
Subset 2	24	27	13	4	0	0
Subset 3	36	16	15	5	2	5
Subset 4	24	11	10	3	2	1
	# of AII tra. branch	Total AII tra branch length (μm)	# of col. plaques	# of col. plaques at tra. crossings	Pl. density	
Subset 1	10	322.9	125	43	0.52	
Subset 2	14	418.6	164	58	0.53	
Subset 3	11	347.4	135	41	0.51	
Subset 4	12	407.9	106	48	0.38	

app str. apposing structure, *prox*. proximal, *dt*. dendrite, *lob-app*. lobular appendages, *pl*. plaques, *tra*. transversal, *col*. colocalizing, *wo* without

Giant bistratified BC-flat midget BC contacts

Giant bistratified BCs possessed long horizontally extending axonal processes in both the OFF and ON sublaminas that allowed for the formation of physical contacts with a variety of costratifying BC subtypes. The PV/Rec/Cx36 triple-stained specimen provided data for such potential interactions for giant bistratified BCs and flat midget BCs in the OFF sublamina. In fact most examined whole mount specimen displayed a costratification of giant bistratified BC and flat midget BC axons in the OFF sublamina (Fig. 7a, b). Moreover, giant bistratified BC and flat midget BC axonal processes tended to sprout in the same IPL location suggesting that they share not only similar horizontal IPL strata but also the vertical information streams. When the giant bistratified BC-flat midget BC physical contacts were examined closely, occasional axo-axonal contact sites (1 such contact out of $n = 6$ was also reconstructed flat midget BC and 4 contacts out of $n = 3$ reconstructed giant bistratified BC were found; see Table 5) contained Cx36 plaques as well (Fig. 7c–h). These putative heterologous BC-to-BC GJ sites were formed by mid-axonal areas of both giant bistratified BCs and flat midget BCs while the tip-to-tip configuration was rare. These GJ sites most often were formed by juxta-varicosity Cx36 plaques on the flat midget BC side, whereas axonal varicosity could not been observed at the giant bistratified BC side (Fig. 6; also see above).

Giant bistratified BC-diffuse type 3 BC and giant bistratified BC-diffuse type 6 contacts

Human giant bistratified BC axons stretched as distal as stratum 4 of the ON sublamina and gave off collaterals in both the ON and OFF layers. This quasi bistratification allowed for the examination of giant bistratified BC-diffuse type 3 BC and giant bistratified BC-diffuse type 6 physical contacts in the PV/CaB/Cx36 specimen for Cx36 plaque colocalizations in both the OFF and ON sublaminas, respectively. CaB + diffuse type 3 BC axons in the OFF sublamina were often found in the vicinity of giant bistratified BC axons (Fig. 8a, b). Reconstructed giant bistratified BCs displayed numerous physical contacts with CaB + profiles

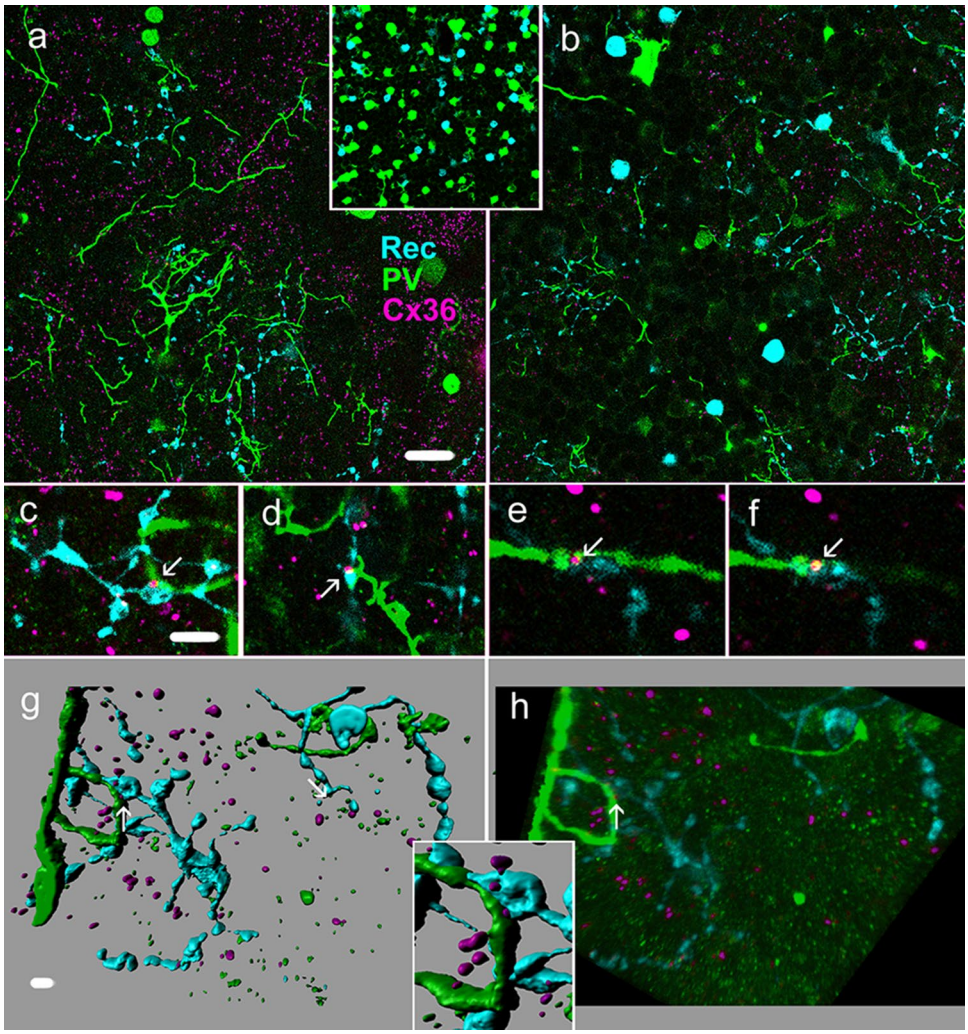

Fig. 7 Cx36 plaques form heterologous BC-to-BC GJs in the inner retina. **a, b** An image pair of the whole mount retina focusing on stratum 1 (**b**) and stratum 2 (**a**) of the specimen displaying giant bistratified BC (GBB; *green*) and flat midget BC (FMB; *turquoise*) axonal processes as well as Cx36 (*magenta*) plaques. Costratification and juxtaposition of giant bistratified BC and flat midget BC axons are evident in both OFF layer strata. *Inset* is taken from a different retinal location with a focus on giant bistratified BC and flat midget BC somata in the INL. **c–f** High power images exhibit Cx36 colocalizations with axonal contact surfaces of giant bistratified BC and flat midget BC cells (*arrows*). **g–h** Imaris reconstruction and corresponding pseudo-confocal image pair display physical juxtaposition of giant bistratified BC (*green*) and flat midget BC (*turquoise*) axons (**g**) with occasional colocalizations (*arrow*) of such contact surfaces with Cx36 plaques (**h**, *arrow*). *Scale bars* **a, b** *inset* 10 µm, **c–h** 2 µm

(mean = 23 ± 9.5 SD). Although, PV/CaR/CaB/Cx36 quadruple labels were not performed to distinguish between sole CaB + diffuse type 3 BC axons and CaR/CaB + AII lobular dendrites we assumed that AII cells do not form electrical synapses with OFF BCs. Thus, the majority (if not all) of PV+/CaB+/Cx36 triple colocalizations were attributed to the presence of giant bistratified BC-diffuse type 3 BC electrical synapses (Fig. 8c, d). Each reconstructed giant bistratified BC formed 0–4 (mean = 2 ± 1.5 SD; see Table 5) such heterologous sites with diffuse type 3 BC axons. Giant bistratified BC axons in the ON sublamina costratified within CaB + diffuse type 6 processes and intermittently they appeared in intimate physical proximity. Many of these contacts beared with colocalizing Cx36 plaques as well (Fig. 8e–g). However, only a PV/CaR/CaB/Cx36 quadruple labeled material would allow for the unequivocal distinction of diffuse type 6 axons and AII cell transversal dendrites thereby detecting giant bistratified BC-diffuse type 6 axonal crossings with colocalizing Cx36 plaques. As this experiment was not feasible in the utilized experimental paradigm, a corresponding quantification was not carried out.

Discussion

The Cx36 antisera used in the present study have been tested in various mamalian species for both specificity and cross-reactions (O'Brien et al. 2012; Rash et al. 2012; Pereda et al. 2003; Kovács-Öller et al. 2014; Völgyi et al. 2013b; Kántor et al. 2016a). Therefore, the punctuate plaque staining in the human inner retina of this study was considered to stain local aggregations of Cx36 subunits. On the other hand, it is obvious that they represent only a fraction of Cx36 plaques in the tissue since smaller aggregates may not be resolved due to the limitations of confocal microscopy (Marc et al. 2013). The positive Cx36 plaque staining, thus represent only the fraction of Cx36 GJs in the human inner retina, whose spatial dimensions were large enough (typically > 200 nm in diameter) for light

Table 5 Colocalization data of reconstructed giant bistratified BC and flat midget BC cells in the human retina

	# of Cx36 plaques	# of Cx36 plaques at FMB/FMB cross	# of FMB/GBB cross. no plaque	# of FMB/GBB cross w Cx36 plaque	# of FMB/PV GC cross no plaque	# of FMB/PV AC cross no plaque	# of FMB/PV AC cross w. Cx36 plaque
FMB(1)	18	0	2	1	8	0	0
FMB(2)	20	0	0	0	1	0	0
FMB(3)	17	0	1	0	3	0	0
FMB(4)	19	0	0	0	2	4	3
FMB(5)	20	0	1	0	2	5	3
FMB(6)	18	0	0	0	0	0	0
FMB mean	18.7 ± 1.2 SD	0	0.7 ± 0.8 SD	0.2 ± 0.4 SD	2.7 ± 2.8 SD	1.5 ± 2.3 SD	1 ± 1.5 SD
	# of Cx36 plaques	# of GBB-GBB contacts no plaque	# of GBB/FMB cross. no plaque	# of GBB/FMB cross w Cx36 plaque	# of GBB/PV GC cross no plaque	# of GBB/PV GC cross w Cx36 plaque	
GBB(1)	17	1	6	1	4	1	
GBB(2)	6	0	6	1	0	0	
GBB(3)	7	1	7	2	0	0	
GBB mean	10 ± 6.1 SD	0.7 ± 0.6 SD	6.3 ± 0.6 SD	1.3 ± 0.6 SD	1.3 ± 2.3 SD	0.3 ± 0.6 SD	
	# of Cx36 plaques	# of GBB-GBB contacts no plaque	# of GBB/DB3 cross. no plaque	# of GBB/DB3 cross w Cx36 plaque	# of GBB/PV GC cross no plaque	# of GBB/PV GC cross w Cx36 plaque	
GBB(4)	14	0	31	4	1	0	
GBB(5)	1	0	33	1	1	0	
GBB(6)	6	1	9	1	0	0	
GBB(7)	2	0	16	3	0	0	
GBB(8)	12	2	29	3	0	0	
GBB(9)	2	0	20	0	0	0	
GBB mean	6.2 ± 5.6 SD	0.5 ± 0.8 SD	23 ± 9.5 SD	2 ± 1.5 SD	0.3 ± 0.5 SD	0	

cross. crossing, *w*. with

microscopic observations. It is expected that future super-resolution light microscopic and electronmicroscopic studies will describe further, yet undetected Cx36 GJ sites in the human retina. Presently, however, the observed Cx36 contacts of this study reveal a number of interesting functional details on signaling in the human retina.

Cx36 expressed by neurons of rod signaling pathways in the human retina

It has been well established that retinal neurons of rod signaling pathways form a number of well described GJs in all examined mammalian species (Deans et al. 2002; Mills et al. 2001; Völgyi et al. 2004, 2013a; Bloomfield and Völgyi 2009). In this study, PKC_{α} and CaR/CaB dual stainings were used to specifically label primary rod pathway RBs and AII cells, respectively. In addition, a cohort of BCs that are potentially postsynaptic to AII ACs and transmit rod signals towards GCs were also stained, including diffuse type 3 BC, diffuse type 6, flat midget BC and giant bistratified BCs. This offered an opportunity to examine if the human retina follows the general mammalian scheme, in which neurons of the primary rod pathway express Cx36 to form GJs for vertical signaling. Although, RBs do not express GJs (Famiglietti and Kolb 1975; Nelson 1982; Vaney 1997; Li et al. 2002) results of this study showed a number of juxtapositions and overlaps of RB axons and Cx36 stained AII transversal processes. Moreover, AII cell dendrites colocalized with the majority of Cx36 plaques that were juxtaposed to RB axons. This indicates that RB-to-AII chemical synapses are strategically positioned in the vicinity of AII GJs thereby facilitating the signal flow along the RB-AII-ON cone BC axis. In fact, diffuse type 6 and ON stratifying giant bistratified BC axons displayed physical contacts with AII transversal processes, many of these contacts possessed Cx36 plaques as well. Therefore, the two neurochemically identified ON signaling cone BCs of this study were clearly postsynaptic to AII cells via Cx36 GJs suggesting that the overall design of the human rod signaling system is similar to those of other mammalian species. This was further confirmed by the presence

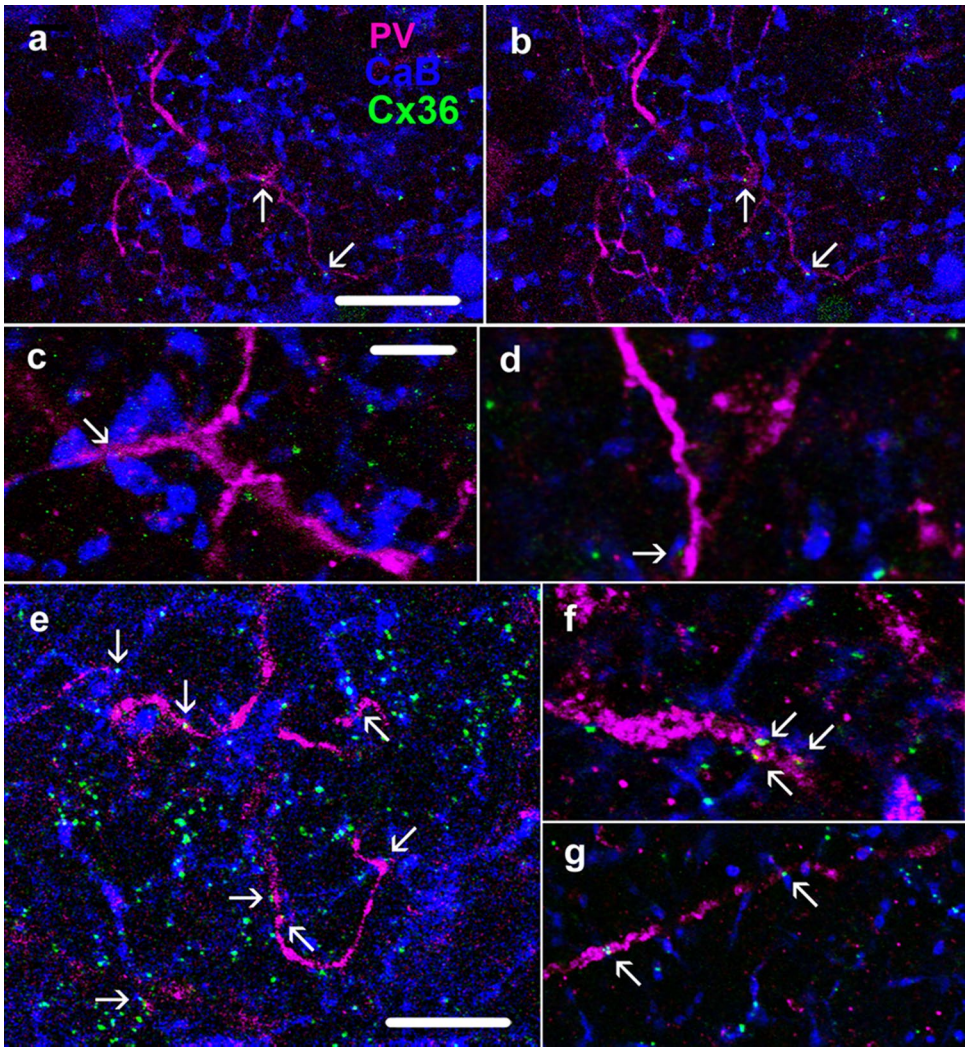

Fig. 8 Heterologous Cx36 GJs formed by blue cone specific giant bistratified BC cells (GBB). **a, b** Image pair showing PV + giant bistratified BC axonal branches (*magenta*), Cx36 plaques (*green*) and CaB + profiles (*blue*) in the OFF sublamina in a whole mount specimen. Occasional colocalizations of Cx36 plaques and axonal contacts of CaB + profiles with giant bistratified BC axons were apparent (*arrows*) suggesting the presence of heterologous giant bistratified BC GJs. **c, d** High magnification images show Cx36 plaques locating in contact sites of giant bistratified BC axons and CaB + profiles in the OFF sublamina. **e–g** Giant bistratified BC axons (*magenta*) in the ON sublamina very often form physical contacts with CaB labeled profiles. The majority of these heterologous contacts are certainly conventional AII-to-ON cone bipolar cell GJs but some of them might be heterologous giant bistratified BC-to-diffuse type 6 GJ contacts. *Scale bars* **a, b, e** 10 µm, **c, d, f, g** 2 µm

of flat midget BC and diffuse type 3 BC axons in the OFF sublamina that displayed close physical contacts with AII lobular dendrites and likely represented glycinerg AII-to-OFF cone BC synapses. Besides the above classic sites, other, unconventional AII cell contacts were also observed. The most numerous were the population of Cx36 plaques that colocalized with the basal surface of AII somata or with emerging primary dendritic areas. As most of these sites showed no observable postsynaptic counterpart it is unclear if they represent unfunctional plaques, hemichannels or GJs with yet undetected neuron profiles. Another curious finding was the population of Cx36 plaques at AII/diffuse type 3 BC contact surfaces. AII cells have been shown to provide glycinergic inhibition to OFF BCs but they have never been shown to exhibit tracer coupling besides nearby AII cells and ON cone BCs (Bloomfield and Dacheux 2001). Thus, if these latter plaques represent GJs they probably serve rectifying GJ contacts in which no tracer or current flows from AII cells to diffuse type 3 BC BCs.

Multiple sites of BC GJs in the mammalian retina

It has been demonstrated that both non-mammalian and mammalian BC neighbors display electrotonic coupling (Van Haesendonck and Missotten 1983; Arai et al. 2010; Marc et al. 1988; Raviola and Gilula 1975; Cohen and Sterling 1990; Vaney 1997; Mills 1999). Some of these contacts occur in the outer retina where GJs form dendritic tip-to-tip contact sites (Raviola and Gilula 1975), whereas others connect BC axonal processes in the inner retina (Marc et al. 1988). Human outer retinal BC GJ subpopulations have recently been reported (Kántor et al. 2016a) and here a cohort of evidence for the existence of human inner retinal BC GJs were presented. Four subtypes of human retinal BCs including flat midget BC, diffuse type 3 BC, diffuse type 6 and giant bistratified BCs were examined in this study and all of them displayed colocalizations with Cx36 plaques along their axons and axonal terminals. Previous results combined with new findngs here indicate that diffuse type 3 BC cell possess several GJ subpopulations.

In the outer retina, diffuse type 3 BC dendritic tips partake in subpedicle Cx36 conglomerates, thick lower order dendrite branches form a second set of Cx36 contacts (Kántor et al. 2016a) and diffuse type 3 BC axons in the inner retina express Cx36 plaques as well. Similarly, flat midget BCs establish both subpedicle and lower order dendritic GJs in the OPL (Kántor et al. 2016a) as well as both homologous and heterologous axonal GJs in the IPL. These results thus provide converging evidence that human BCs may in fact form four distinct sets of GJs, including subpedicle dedritic tip-to-tip GJs and lower order dendrodendritic GJs in the outer retina, as well as homologous and heterologous axo-axonal GJs in the inner retina. The fact that representative parvo-, magno- and koniocellular pathway BCs share this feature suggests that GJ coupling of BCs is general and likely serve all vertical signaling pathways in the human retina.

Function of GJ coupling in vertical signaling

We found that axons of four cone BC types displayed colocalizations with Cx36 plaques. Flat midget BC axons arborize in strata 1 and 2 of the IPL. Contrary to the presence of relative few Cx36 plaques in these strata and the low number of flat midget BC terminals, a number of their axons exhibited colocalizations with Cx36 plaques. A few of these occured at close appositions of BC-to- BC contact sites suggesting that flat midget BCs maintain a homologously coupled array in the OFF sublamina. Similar evidence for homologous BC-to-BC GJs were found for diffuse type 3 and diffuse type 6 axons as well. Interestingly, giant bistratified BC axons did not seem to contact one another thus leaving little (or no) chance for homologous Cx36 GJs. The homologous coupling of primate diffuse BCs have previously been reported (Luo et al. 1999; Dacey et al. 2000) and results of this study now provide evidence for similar interactions in the human retina as well. Interestingly, however, such putative homologous sites were relatively rare compared to the frequency of Cx36 colocalizations with BC markers. Therefore, most BC GJs observed in this study likely represent heterologous contacts with other inner retinal cell types. As no AC-to-BC or GC-to-BC GJs have been reported in animal models (besides the well known AII AC-to-ON BC contacts) the above finding indicates that dissimilar BC subtypes form functional GJs in the human retina. The existence of such heterologous BC GJs have been reported in lower vertebrates (Marc et al. 1988) and non-primate mammals (Mills 1999), however, this is the first study to report on this phenomenon in the human retina. The relative large number of such colocalizing Cx36 plaques reflects not simply the existece but also the dominance of heterologous BC GJs. As same-type BCs tile the retinal surface economically, only tip-to-tip axonal contacs allow for homologous BC coupling. Thus, the presented finding here, to show that Cx36 plaques prefered mid-axonal locations over axon terminals further supports the heterologous BC-to-BC GJ dominancy hypothesis. In fact, occasional Cx36 plaques occurred at close appositions of flat midget and giant bistratified BCs. A somewhat more frequent colocalization of Cx36 was detected at physical contacts that occurred between giant bistratified BCs and CaB + profiles that likely represented diffuse type 3 BC and diffuse type 6 BC axon crossings. It has been put forward that BC-to-BC electrotonic coupling may decrease the dispersion of BC input signals to respond uniformly to light (Umino et al. 1994; Jacobs and Werblin 1998). According to a very recent study, the lateral spread of signals through electrically coupled BCs contributed to a nonlinear enhancement of BC output in the mouse retina (Kuo et al. 2016). Such enhacement occurred when paired stimuli were presented close in both space and time, thus suggesting that BC GJs increase GC sensitivity to spatiotemporally correlated inputs. While homologous BC GJ contacts may serve these functions, the purpose of heterologous BC GJ connections is certainly different from that. Most likely, heterologous GJs underly an intermixing of information carried by parallel retinal pathways.

Intermixing of BC information streams

Although, the existence of BC GJs have been repeatedly reported in animal models, this study on the human retina reveals a number of unexpected details regarding this issue. First, though with different rates, all major retinal information streams seem to contribute to BC GJ signaling. This finding may not be discomforting for magnocellular pathway, in which stream parasol GCs have large non-color sensitive receptive fields and summate inputs from different BC types. For example, OFF parasol cells receive inputs from diffuse type 2 and diffuse type 3 BCs (Jacoby and Marshak 2000; Tsukamoto and Omi 2015; Masri et al. 2016), whereas ON parasol cells are postsynaptic to diffuse type 4 and diffuse type 5 cells (Jacoby et al. 1996; Marshak et al. 2002). Thus, homologous GJ coupling of diffuse type 3 BCs observed here may serve saliency of information processing. Diffuse type 6 axons costratify with dendrites of various GC types, including small bistratified, large bistratified, melanopsin-immunoreactive and monostratified GCs (Ghosh et al. 1997; Dacey et al. 2000, 2003; Jusuf et al. 2004) but only large sparse GCs have been confirmed to be postsynaptic to diffuse type 6 cells (Percival et al. 2011). These latter diffuse type 6 recipient GCs do not process high contrast visual signals, thus homologous coupling of koniocellular diffuse type 6 cells might be adventageous for these GCs as well. However, parvocellular pathway specific OFF flat midget BCs appeared to display the highest

density of colocalizing Cx36 plaques. It is hard to explain why high contrast visual information conveying flat midget BCs form GJs to signal laterally, and therefore, potentially perturbing high acuity vision. However, most flat midget BC GJs are not homologous thus flat midget BCs do not communicate with their neighbors to compromize high visual acuity. These GJs rather serve to send flat midget BC signals to a parallel non-high acuity retinal pathway(s). Hereby two alternative hypotheses are provided to explain the function of heterologous GJs between parvocellular flat midget BCs and blue cone pathway giant bistratified BCs. In the first scheme, flat midget BCs serve a dual functional role. First, they deliver high contrast color opponent information to midget GCs through the conventional cone-flat midget BC-OFF midget GC pathway. In addition, they also provide indirect input to small-bistratified GCs (and likely large bistratified also) to create their (L + M) OFF center responses (Dacey et al. 2014). According to our hypothesis flat midget BC signal is passed to giant bistratified BCs via GJs for signal averaging prior transmission to bistratified GCs. This circuit thus allows for an averaging of flat midget BC signals transmitted to small-bistratified GCs but keeping flat midget BC signals segregated for midget GCs (see Online Resource 5).

According to another hypothesis activation evoked currents of flat midget BCs are sinked by GJ coupled giant bistratified BCs thereby impeding flat midget BC-to-midget GC signaling. In this case, only strong contrast-initiated high amplitude flat midget BC depolarizations pass all GJ sinks, reach presynaptic axonal sites and then ultimately are translated to midget GC signal. On the other hand, weaker BC currents are sinked by heterologous GJs and postsynaptic GCs remain unaffected by the signal. On the other hand, when coupled flat midget BCs and giant bistratified BCs are depolarized by the same visual stimulus and they are on equipotential the sinking mechanism does not take place. Large field giant bistratified BCs could be depolarized effectively only by a larger object/stimulus. Therefore, such mechanism may tune visual acuity to percieve small objects against high contrast background, and low contrasts are only translated to GC signals if they reach a certain size (Online Resource 5). If this mechanism exists it can save the visual system from transmitting information of featurless noise stimuli from the retina to the brain. The fact that Cx36 plaques were often found in a juxtaposition to flat midget BC varicosities, the chemical output sites to postsynaptic GCs, may support this hypothesis. That is, a GJ mediated sinking mechanism is more effective if it takes place near the BC output.

BCs in the human retina consist of some 10–12 cell types, most of which have morphological homologs in other examined mammalian species: (1) the human and monkey diffuse type 3 BCs show remarkable morphological similarities with mouse and rat type 5 and rabbit CBa2n cells; (2) flat midget BCs appear homologous to type 2 in rat and mouse as well as CBa1-2 BCs in the rabbit retina; (3) human diffuse type 6 BCs are homologous with mouse and rat type 8 cells and rabbit CBb5 cells and (4) giant bistratified bipolar cells share many morphological features with wide-field BCs in the rabbit retina and shows similarities with type 9 cells in the rat and the mouse (Kolb et al. 1992; Haverkamp et al. 2003; Ghosh et al. 2004; Jusuf et al. 2004; Masland 2011; Kántor et al. 2016a, b). Although, future studies have to reinforce that these morphological similarities correspond to functional homologies as well it is very likely that the above hypothetical functions allocated to human BC GJs are consistent among mammalian species.

Acknowledgements Supported by OTKA K105247 to B. V. and by the Hungarian Brain Research Program (KTIA_NAP_13-2-2015-0008) to B. V. This research was also supported by the European Union and the State of Hungary, co-financed by the European Social Fund in the framework of TÁMOP- 4.2.4.A/2–11/1-2012-0001 'National Excellence Program' to B. V. The technical assistance of Zsuzsanna Vidra is gratefully appreciated. The authors are thankful to Wilhelm Koch providing the recoverin anibody.

References

Alonso JM, Usrey WM, Reid RC (1996) Precisely correlated firing in cells of the lateral geniculate nucleus. Nature 383:815–819

Arai I, Tanaka M, Tachibana M (2010) Active roles of electronically coupled bipolar cell network in the adult retina. J Neurosci 30:9260–9270. doi:10.1523/JNEUROSCI.1590-10.2010

Bloomfield SA, Dacheux RF (2001) Rod vision: pathways and processing in the mammalian retina. Prog Retin Eye Res 20:351–384

Bloomfield SA, Völgyi B (2009) The diverse functional roles and regulation of neuronal gap junctions in the retina. Nat Rev Neurosci 10:495–506. doi:10.1038/nrn2636

Chen YY, Liu SL, Hu DP, Xing YQ, Shen Y (2014) *N*-methyl-*N*-nitrosourea induced retinal degeneration in mice. Exp Eye Res 121:102–113. doi:10.1016/j.exer.2013.12.019

Cohen E, Sterling P (1990) Cenvergence and divergence of cones onto bipolar cells in the central area of cat retina. Philos Trans R Soc Lond B Biol Sci 330:323–328

Dacey D, Packer OS, Diller L, Brainard D, Peterson B, Lee B (2000) Center surround receptive field structure of cone bipolar cells in primate retina. Vision Res 40:1801–1811

Dacey DM, Peterson BB, Robinson FR, Gamlin PD (2003) Fireworks in the primate retina: in vitro photodynamics reveals diverse LGN-projecting ganglion cell types. Neuron 37:15–27

Dacey DM, Crook JD, Packer OS (2014) Distinct synaptic mechanisms create parallel S-ON and S-OFF color opponent pathways in the primate retina. Vis Neurosci 31:139–151. doi:10.1017/S0952523813000230

Deans MR, Völgyi B, Goodenough DA, Bloomfield SA, Paul DL (2002) Connexin36 is essential for transmission of rod-mediated visual signals in the mammalian retina. Neuron 36:703–712

Eliasieh K, Liets LC, Chalupa LM (2007) Cellular reorganization in the human retina during normal aging. Invest Ophthalmol Vis Sci 48:2824–2830

Famiglietti EV, Kolb H (1975) A bistratified amacrine cell and synaptic circuitry in the inner plexiform layer of the retina. Brain Res 84:293–300

Feigenspan A, Teubner B, Willecke K, Weiler R (2001) Expression of neuronal connexin36 in AII amacrine cells of the mammalian retina. J Neurosci 21:230–239

Feigenspan A, Janssen-Bienhold U, Hormuzdi S, Monyer H, Degen J, Söhl G, Willecke K, Ammermüller J, Weiler R (2004) Expression of connexin36 in cone pedicles and OFF-cone bipolar cells of the mouse retina. J Neurosci 24:3325–3334

Ghosh KK, Martin PR, Grünert U (1997) Morphological analysis of the blue cone pathway in the retina of a New World monkey, the marmoset Callithrix jacchus. J Comp Neurol 379:211–225

Ghosh KK, Bujan S, Haverkamp S, Feigenspan A, Wässle H (2004) Types of bipolar cells in the mouse retina. J Comp Neurol 469:70–82

Grünert U, Martin PR, Wässle H (1994) Immunocytochemical analysis of bipolar cells in the macaque monkey retina. J Comp Neurol 348:607–627

Güldenagel M, Söhl G, Plum A, Traub O, Teubner B, Weiler R, Willecke KS (2000) Expression patterns of connexin genes in mouse retina. J Comp Neurol 425:193–201

Güldenagel M, Ammermüller J, Feigenspan A, Teubner B, Degen J, Söhl G, Willecke K, Weiler R (2001) Visual transmission deficits in mice with targeted disruption of the gap junction gene connexin36. J Neurosci 21:6036–6044

Han Y, Massey SC (2005) Electrical synapses in retinal ON cone bipolar cells: subtype-specific expression of connexins. PNAS 102:13313–13318

Haverkamp S, Haeseleer F, Hendrickson A (2003) A comparison of immunocytochemical markers to identify bipolar cell types in human and monkey retina. Visual Neurosci 20:589–600

Hidaka S, Akahori Y, Kurosawa Y (2004) Dendrodendritic electrical synapses between mammalian retinal ganglion cells. J Neurosci 24:10553–10567

Hombach S, Janssen-Bienhold U, Söhl G, Schubert T, Büssow H, Ott T, Weiler R, Willecke K (2004) Functional expression of connexin57 in horizontal cells of the mouse retina. Eur J Neurosci 19:2633–2640

Hunyady B, Krempels K, Harta G, Mezey E (1996) Immunohistochemical signal amplification by catalyzed reporter deposition and its application in double immunostaining. J Histochem Cytochem 44:1353–1362

Jacobs AL, Werblin FS (1998) Spatiotemporal patterns at the retinal output. J Neurophysiol 80:447–451

Jacoby RA, Marshak DW (2000) Synaptic connections of DB3 diffuse bipolar cell axons in macaque retina. J Comp Neurol 416:19–29

Jacoby R, Stafford D, Kouyama N, Marshak D (1996) Synaptic inputs to ON parasol ganglion cells in the primate retina. J Neurosci 16:8041–8056

Jacoby RA, Wiechmann AF, Amara SG, Leighton BH, Marshak DW (2000) Diffuse bipolar cell provide input to OFF parasol ganglion cells in the macaque retina. J Comp Neurol 416:6–18

Jusuf PR, Lee SCS, Grünert U (2004) Synaptic connectivity of the diffuse bipolar cell type DB6 in the inner plexiform layer of primate retina. J Comp Neurol 469:494–506

Kántor O, Benkő Z, Énzsöly A, Dávid C, Naumann A, Nitschke R, Szabó A, Pálfi E, Orbán J, Nyitrai M, Németh J, Szél Á, Lukáts Á, Völgyi B (2016a) Characterization of connexin36 gap junctions in the human outer retina. Brain Struct Funct 221:2963–2984. doi:10.1007/s00429-015-1082-z

Kántor O, Mezey S, Adeghate J, Naumann A, Nitschke R, Énzsöly A, Szabó A, Lukáts Á, Németh J, Somogyvári Z, Völgyi B (2016b) Calcium buffer proteins are specific markers of human retinal neurons. Cell Tissue Res 365:29–50. doi:10.1007/s00441-016-2376-z

Kántor O, Varga A, Tóth R, Énzsöly A, Pálfi E, Kovács-Öller T, Nitschke R, Szél Á, Székely A, Völgyi B, Négyessy L, Somogyvári Z, Lukáts Á (2015) Stratified organization and disorganization of inner plexiform layer revealed by TNAP activity in healthy and diabetic rat retina. Cell Tissue Res 359(2):409–421. doi:10.1007/s00441-014-2047-x

Kihara AH, Mantovani de Castro L, Belmonte MA, Yan CY, Moriscot AS, Hamassaki DE (2006) Expression of connexins 36, 43, and 45 during postnatal development of the mouse retina. J Neurobiol 66:1397–1410

Kihara AH, Santos TO, Osuna-Melo EJ, Paschon V, Vidal KS, Akamine PS, Castro LM, Resende RR, Hamassaki DE, Britto LR (2010) Connexin-mediated communication controls cell proliferation and is essential in retinal histogenesis. Int J Dev Neurosci 28:39–52. doi:10.1016/j.ijdevneu.2009.09.006

Kolb H, Linberg KA, Fischer SK (1992) Neurons of the human retina: A Golgi study. J Comp Neurol 318:147–187

Kovács-Öller T, Debertin G, Raics K, Orbán J, Nyitrai M, Völgyi B (2014) Developmental changes in the expression level of connexin36 in the rat retina. Cell Tissue Res 358:289–302. doi:10.1007/s00441-014-1967-9

Kuo SP, Schwartz GW, Rieke F (2016) Nonlinear spatiotemporal integration by electrical and chemical synapses in the retina. Neuron 90:320–332. doi:10.1016/j.neuron.2016.03.012

Lee EJ, Han JW, Kim HJ, Kim IB, Lee MY, Oh SJ, Chung JW, Chun MH (2003) The immunocytochemical localization of connexin 36 at rod and cone gap junctions in the guinea pig retina. Eur J Neurosci 18:2925–2934

Lee SC, Weltzien F, Madigan MC, Martin PR, Grünert U (2016) Identification of AII amacrine, displaced amacrine, and bistratified ganglion cell types in human retina with antibodies against calretinin. J Comp Neurol 524:39–53. doi:10.1002/cne.23821

Li W, Zhang J, Massey SC (2002) Coupling pattern of S1 and S2 amacrine cells in the rabbit retina. Vis Neurosci 19(2):119–131

Lin B, Jakobs TC, Masland RH (2005) Different functional types of bipolar cells use different gap- junctional proteins. J Neurosci 25:6696–6701

Luo X, Ghosh KK, Martin PR, Grünert U (1999) Analysis of two types of cone bipolar cells in the retina of a New World monkey, the marmoset, Callithrix jacchus. Vis Neurosci 16:707–719

Marc RE, Liu WL, Müller JF (1988) Gap junctions in the inner plexiform layer of the goldfish retina. Vision Res 28:9–24

Marc RE, Jones BW, Watt CB, Anderson JR, Sigulinsky C, Lauritzen S (2013) Retinal connectomics: towards complete, accurate networks. Prog Retin Eye Res 37:141–162. doi:10.1016/j.preteyeres.2013.08.002

Marshak DW, Yamada ES, Bordt AS, Perryman WC (2002) Synaptic input to an ON parasol ganglion cell in the macaque retina: a serial section analysis. Vis Neurosci 19:299–305

Masland D (2011) Cell Populations of the retina: the proctor lecture. Investig Ophthalmol Vis Sci 52:4581–4591

Masri RA, Percival KA, Koizumi A, Martin PR, Grünert U (2016) Connectivity between the OFF bipolar type DB3a and six types of ganglion cell in the marmoset retina. J Comp Neurol 524:1839–1858. doi:10.1002/cne.23925

Massey SC, O'Brien JJ, Trexler EB, Li W, Keung JW, Mills SL, O'Brien J (2003) Multple neuronal connexins in the mammalian retina. Cell Commun Adhes 10:425–430

Maxeiner S, Dedek K, Janssen-Bienhold U, Ammermüller J, Brune H, Kirsch T, Pieper M, Degen J, Krüger O, Willecke K, Weiler R (2005) Deletion of connexin45 in mouse retinal neurons disrupts the rod/cone signaling pathway between AII amacrine and ON cone bipolar cells and leads to impared visual transmission. J Neurosci 25:566–576

Mills SL (1999) Unusual coupling patterns of a cone bipolar cell in the rabbit retina. Vis Neurosci 16:1029–1035

Mills SL, O'Brien JJ, Li W, O'Brien J, Massey SC (2001) Rod pathways in the mammalian retina use connexin36. J Comp Neurol 436:336–350

Müller LP, Dedek K, Janssen-Bienhold U, Meyer A, Kreuzberg MM, Lorenz S, Willecke K, Weiler R (2010) Expression and modulation of connexin 30.2, a novel gap junction protein in the mouse retina. Vis Neurosci 27:91–101. doi:10.1017/S0952523810000131

Nelson R (1982) AII amacrine cells quicken time course of rod signals in the cat retina. J Neurophysiol 47:928–947

O'Brien JJ, Chen X, Macleish PR, O'Brien J, Massey SC (2012) Photoreceptor coupling mediated by connexin36 in the primate retina. J Neurosci 32:4675–4687. doi:10.1523/JNEUROSCI.4749-11.2012

Pan F, Paul DL, Bloomfield SA, Völgyi B (2010) Connexin36 is required for gap junctional coupling of most ganglion cell subtypes in the mouse retina. J Comp Neurol 518:911–927. doi:10.1002/cne.22254

Percival KA, Martin PR, Grünert U (2011) Synaptic inputs to two types of koniocellular pathway ganglion cells in marmoset retina. J Comp Neurol 519:2135–2153. doi:10.1002/cne.22586

Percival KA, Martin PR, Grünert U (2013) Organisation of koniocellular-projecting ganglion cells and diffuse bipolar cells in the primate fovea. Eur J Neurosci 37:1072–1089. doi:10.1111/ejn.12117

Percival KA, Koizumi A, Masri RA, Buzás P, Martin PR, Grünert U (2014) Identification of a pathway from the retina to koniocellular layer K1 in the lateral geniculate nucleus of marmoset. J Neurosci 34:3821–3825. doi:10.1523/JNEUROSCI.4491-13.2014

Pereda A, O'Brien JO, Nagy JI, Bukauskas F, Davidson KGV, Kamasawa N, Yasumura T, Rash JE (2003) Connexin35 mediates electrical transmission at mixed synapses on Mauthner cells. J Neurosci 23:7489–7503

Petrasch-Parwez E, Habbes HW, Weickert S, Löbbecke-Schumacher M, Striedinger K, Wieczorek S, Dermietzel R, Epplen JT (2004) Fine-structural analysis and connexin expression in the retina of a transgenic model of Huntington's disease. J Comp Neurol 479:181–197

Puthussery T, Gayet-Primo J, Taylor WR (2010) Localization of the calcium-binding protein secretagogin in cone bipolar cells of the mammalian retina. J Comp Neurol 518:513–525. doi:10.1002/cne.22234

Rash JE, Kamasawa N, Davidson KGV, Yasumura T, Pereda AE, Nagy JI (2012) Connexin composition in apposed gap junction hemiplaques revealed by matched double-replica freeze-fracture replica immunogold labeling. J Membr Biol 245:333–344. doi:10.1007/s00232-012-9454-2

Raviola E, Gilula NB (1975) Intramembrane organization of specialized contacts in the outer plexiform layer of the retina. A freeze-fracture study in monkeys and rabbits. J Cell Biol 65:192–222

Regus-Leidig H, Specht D, Tom Dieck S, Brandstätter JH (2010) Stability of active zone components at the photoreceptor ribbon complex. Mol Vis 16:2690–2700

Regus-Leidig H, Fuchs M, Löhner M, Leist SR, Leal-Ortiz S, Chiodo VA, Hauswirth WW, Garner CC, Brandstätter JH (2014) In vivo knockdown of Piccolino disrupts presynaptic ribbon morphology in mouse photoreceptor synapses. Front Cell Neurosci 8:259. doi:10.3389/fncel.2014.00259

Schindelin J, Arganda-Carreras I, Frise E, Kaynig V, Longair M, Pietzsch T, Preibisch S, Rueden C, Saalfeld S, Schmid B et al (2012) Fiji: an open-source platform for biological-image analysis. Nat Methods 9:676–682. doi:10.1038/nmeth.2019

Schubert T, Degen J, Willecke K, Hormuzdi SG, Monyer H, Weiler R (2005a) Connexin36 mediates gap junctional coupling of alpha-ganglion cells in mouse retina. J Comp Neurol 485:191–201

Schubert T, Maxeiner S, Krüger O, Willecke K, Weiler R (2005b) Connexin45 mediates gap junctional coupling of bistratified ganglion cells in the mouse retina. J Comp Neurol 490:29–39

Söhl G, Joussen A, Kociok N, Willecke K (2010) Expression of connexin genes in the human retina. BMC Ophthalmol 10:27. doi:10.1186/1471-2415-10-27

Toader O, Forte N, Orlando M, Ferrea E, Raimondi A, Baldelli P, Benfenati F, Medrihan L (2013) Dentate gyrus network dysfunctions precede the symptomatic phase in a genetic mouse model of seizures. Front Cell Neurosci 7:138. doi:10.3389/fncel.2013.00138

Tomassy GS, Morello N, Calcagno E, Giustetto M (2014) Developmental abnormalities of cortical interneurons precede symptoms onset in a mouse model of Rett syndrome. J Neurochem 131:115–127. doi:10.1111/jnc.12803

Tsukamoto Y, Omi N (2015) OFF bipolar cells in macaque retina: type-specific connectivity in the outer and inner synaptic layers. Front Neuroanat 9:122 doi:10.3389/fnana.2015.00122

Umino O, Maehara M, Hidaka S, Kita S, Hashimoto Y (1994) The network properties of bipolar-bipolar cell coupling in the retina of teleost fishes. Vis Neurosci 11:533–548

Usrey WM, Reid RC (1999) Synchronous activity in the visual system. Annu Rev Physiol 61:435–456

Van Haesendonck E, Missotten L (1983) Interbipolar contacts in the dorsal inner plexiform layer in the retina of Callionymus lyra L. J Ultrastruct Res 83:303–311

Vaney DI (1997) Neuronal coupling in rod-signal pathways of the retina. Invest Ophthalmol Vis Sci 38(2):267–273

Völgyi B, Deans MR, Paul DL, Bloomfield SA (2004) Convergence and segregation of the multiple rod pathways in mammalian retina. J Neurosci 24:11182–11192

Völgyi B, Abrams J, Paul DL, Bloomfield SA (2005) Morphology and tracer coupling pattern of alpha ganglion cells in the mouse retina. J Comp Neurol 492:66–77

Völgyi B, Chheda S, Bloomfield SA (2009) Tracer coupling patterns of the ganglion cell subtypes in the mouse retina. J Comp Neurol 512:664–687. doi:10.1002/cne.21912

Völgyi B, Kovács-Oller T, Atlasz T, Wilhelm M, Gábriel R (2013a) Gap junctional coupling in the vertebrate retina: variations on one theme? Prog Retin Eye Res 34:1–18. doi:10.1016/j.preteyeres.2012.12.002

Völgyi B, Pan F, Paul DL, Wang JT, Huberman AD, Bloomfield SA (2013b) Gap junctions are essential for generating the correlated spike activity of neighboring retinal ganglion cells. PLoS One 8:e69426. doi:10.1371/journal.pone.0069426

Weltzien F, Dimarco S, Protti DA, Daraio T, Martin PR, Grünert U (2014) Characterization of secretagogin-immunoreactive amacrine cells in marmoset retina. J Comp Neurol 522:435–455. doi:10.1002/cne.23420